NAT'L INST. OF STAND & TECH
A11106 387272
NBS
PUBLICATIONS

NBSIR 80-2181

Measurement Techniques for Solar Cells, Annual Report December 15, 1978 to December 14, 1979

D. E. Sawyer, H. K. Kessler, T. J. Russell,
W. F. Lankford, and H. A. Schafft

Electron Devices Division
Center for Electronics and Electrical Engineering
National Engineering Laboratory
U.S. Department of Commerce
National Bureau of Standards
Washington, DC 20234

January 1981

Prepared for
Solar Energy Research Institute
Golden, CO 80401

QC
100
.U56
80-2181
1981
c. 2

National Bureau of Standards
Library, E-01 Admin. Bldg.
MAR 2 1981
not circ - Ref
QC100
.U56
no 80-2181
1981
c.2

NBSIR 80-2181

MEASUREMENT TECHNIQUES FOR SOLAR CELLS, ANNUAL REPORT DECEMBER 15, 1978 TO DECEMBER 14, 1979

D. E. Sawyer, H. K. Kessler, T. J. Russell,
W. F. Lankford, and H. A. Schafft

Electron Devices Division
Center for Electronics and Electrical Engineering
National Engineering Laboratory
U.S. Department of Commerce
National Bureau of Standards
Washington, DC 20234

January 1981

Prepared for
Solar Energy Research Institute
Golden, CO 80401

U.S. DEPARTMENT OF COMMERCE, Malcolm Baldrige, *Secretary*
NATIONAL BUREAU OF STANDARDS, Ernest Ambler, *Director*

Table of Contents

		Page
1.	Executive Summary	1
2.	Application of the Laser Flying-Spot Scanner to Solar Cells and Materials	3
	2.1 Overview	3
	2.2 Experimental Zinc Phosphide Schottky Diodes	4
	2.3 Silicon Tandem Junction Cells	4
	2.4 Ungridded Cu_2S/CdS Cells	6
	2.5 EFG Polycrystalline Silicon Cells	8
	2.5.1 Defect Location	8
	2.5.2 Silicon Carbide Particles	8
	2.5.3 Crack Parallel to a Metallization Finger	11
	2.5.4 Back Contact Faults	11
	2.5.5 Deliberate Scratches	18
	2.6 New Applications	18
3.	Mathematical Modeling	19
4.	NBS-22, A Solar Cell Test Pattern	19
	4.1 Description of the Pattern	20
	4.2 Sample Preparation and Data Collection	24
5.	Laser Scanner Ancillary Technique and Apparatus Development	24
	5.1 Improved Reflected-Light Detection System	24
	5.1.1 Alignment of Reflected-Light Optical Path	28
	5.1.2 Photomultiplier Detector	30
	5.2 Specimen Birefringence Microscope Attachment	30
	5.3 A Light Source for Biasing Large-Diameter Cells	34
	5.4 Optical Parameters of Various Lens Combinations	35
	5.5 Variable Specimen Temperature	40
	5.5.1 Heating Stage	40
	5.5.2 Cooling Stage, Thermoelectric Type	40
	5.5.3 Cooling Stage, Compressor Type	41
6.	Workshops	43
	6.1 Stability of (Thin Film) Solar Cells and Materials	43
	6.2 Photovoltaic Material and Device Measurements	43
7.	Consultation and Liaison Activities	43
	7.1 Consultations to SERI	43
	7.2 Visits from Industry and Universities to the National Bureau of Standards	44
References		46
Appendix A		48
Appendix B		49

List of Figures

		Page
1.	Sketch of semicircular magnesium metallization contact patterns deposited to form Schottky barriers on *p*-type Zn_3P_2	5
2.	Sketch of a tandem junction solar cell	5
3.	Ungridded Cu_2S/CdS cell response to 0.633-μm scanning light . . .	7
4.	Ungridded Cu_2S/CdS cell response after scratching the surface . .	7
5.	Photoresponse map to 0.633-μm light of an early low-cost EFG cell with 500-mA forward bias	9
6.	Photoresponse of an EFG cell near a silicon carbide particle producing a point shunt through the cell indicated by the reduced signal as the laser spot approaches the particle.	10
7.	Predicted photoresponse of a cell with a point shunt located at 0.5 (dotted lines) compared to a perfect cell (solid lines) . . .	10
8.	Line scan through the region of a cell where a silicon carbide particle is producing a point shunt	12
9.	Line scan in the region of a cell when a silicon carbide particle has not produced a shunt through the cell	12
10.	Raster scan of an EFG cell under a few suns light bias to identify a hairline crack between the second and third metallization finger from the left	13
11.	Line scan of the cracked region of the cell in figure 10	13
12.	Expanded line scan of the previous cell before the crack has spread to the bus bar metallization	14
13.	Same cell as in figure 12 at a later time when the crack has interrupted the flow of current along the bus bar	15
14.	Line scan adjacent to the bus bar showing the reduction in photoresponse due to the crack	15
15.	Photoresponse of a high quality 1-cm by 4-cm EFG cell	16
16.	Cell of figure 15 under about 3 suns light bias	16
17.	Cell of figure 15 under no light bias but with 1.15-μm laser light indicating the photoresponse at the back contact more clearly	17

Page

18. NBS-22 test pattern which includes four solar cells (A, B, C, and D) surrounded by arrays of microelectronic test structures 21

19. Expanded view of the D solar cell which contains the doubly diffused and the singly diffused regions of the cell and also the regions where the metallization does not contact the emitter surface, shown as the white breaks 22

20. The microelectronic test structure pattern which surrounds the solar cell 23

21. Sheet resistance measurement locations around cell A for values given in table 2 27

22. New reflected-light asssembly using a germanium photodiode visible on the right-hand component 29

23. Reflected light configuration with a photomultiplier detector 31

24. Raster scan of most of an NBS-22 solar cell using the configuration of figure 23 in the large area scan mode of figures 25 and 26 32

25. Optical diagram for the large area scan configuration 38

26 Photograph of the large area scan configuration 39

27. Photograph of the compressor type cooling stage (top) and cover (bottom) 42

List of Tables

Page

1. Test Structure List 25

2. Sheet Resistance ± Standard Deviation 26

3. NBS Laser Scanner Specimen to Objective-Lens Working Distance and Scan Excursion for the 0.633-μm Laser Wavelength Tabulated Using a 10X Ocular Lens, a Total Optical Scanning Angle of 20 Deg at the Ocular Lens, and with Various Objective Lenses 36

4. NBS Laser Scanner Scanning Resolution and Reflected-Light Bias, for 0.633- and 1.15-μm Laser Wavelengths Tabulated Using a 10X Ocular Lens and with Various Objective Lenses 37

Disclaimer

Certain commercial equipment, instruments, or materials are identified in this report in order to adequately specify the experimental procedure. In no case does such identification imply recommendation or endorsement by the National Bureau of Standards, nor does it imply that the material or equipment identified is necessarily the best available for the purpose.

Measurement Techniques for Solar Cells

Annual Report
December 15, 1978 to December 14, 1979

D. E. Sawyer,* H. K. Kessler,†
T. J. Russell, W. F. Lankford, and H. A. Schafft

1. EXECUTIVE SUMMARY

This report covers research performed in the period December 15, 1978 to December 14, 1979 on Solar Cell Measurement Technique Development and Other Services by the Electron Devices Division of the National Bureau of Standards (NBS). The objectives of the project are to provide support to the Department of Energy (DoE) thin-film photovoltaic effort in the following ways: (1) by developing solar cell device and measurement techniques using the NBS-developed laser flying-spot scanner and (2) by assisting the DoE in organizing appropriate workshops and symposia and providing general consultation and liaison services.

In this annual report, further applications of the NBS scanning technique are described. The technique has been applied to experimental solar cells and cell prototypes of interest in the Solar Energy Research Institute (SERI) Photovoltaic Program Office (PVPO). Cells and prototypes scanned include Cu_2S/CdS cells, silicon tandem junction cells, Zn_3P_2 Schottky diode specimens, and edge-fed growth (EFG) polycrystalline silicon cells. Scanning of these cells was performed with the cell suppliers present to aid in the rapid transfer of scanning results and dissemination of scanning techniques. For the Cu_2S/CdS cells, the results show that it is possible to screen cells for quality before the most expensive fabrication step, gridding, is performed. For this cell type, the importance of proper handling techniques was underscored by laser scanning an ungridded cell before and after the cell was intentionally damaged by scratching the cell surface. Scanning the tandem junction cells pinpointed a source of cell-efficiency loss and motivated the redesign of the cell. Scanning of the Zn_3P_2 specimens yielded values of the effective minority carrier diffusion length in the Zn_3P_2 in satisfactory agreement with the results obtained using other techniques. The results of scanning the EFG cells were interpreted by the supplier to yield the locations of missing antireflective (AR) coating, metallization finger breaks and loss of ohmic contact of metallization, back contact problems, hairline cracks, and regions having reduced minority carrier lifetime. The electrical effects of silicon carbide inclusions were also observed. Another result of the EFG cell scanning was that the supplier was able to pinpoint a fabrication-related source of excess cell resistance.

---

* Presently employed by Chevron Research Co., Solar Research Division, P. O. Box 1627, Richmond, CA 94802.

† Retired.

The results of the EFG scanning work were interpreted by the supplier as consistent with the first-order mathematical modeling performed by NBS and with the more detailed modeling performed by K. Lehovec and A. Fedotowsky at the University of Southern California as part of this effort. These USC workers have completed a mathematical analysis which shows that the response-equivalency of line and point-light scanning is a general result and holds for cells having defects as well as for perfect cells. Also treated is the scanning response of a cell containing a point short-circuit and a cracked cell having various values of crack shunt conductance with the cell crack both parallel to the metallization fingers and at various angles to the fingers. Although the modeling was based on single-crystal cells, the results are expected to be applicable to other, and more exploratory, cell materials, e.g., polycrystalline silicon: shorts are commonly observed in polycrystalline silicon cells, and some of the effects which can occur at grain boundaries can be modeled in terms of localized junction shunting.

A solar cell test pattern (NBS-22) was conceived and an initial design completed during the previous reporting year (September 15, 1977 to December 14, 1978) with the objective of providing precisely known artifacts to link the solar cell modeling work with cell laser scanning under controlled conditions in order to put laser scanning on a firm theoretical, and reproducible, basis. The final design, fabrication, and initial testing of NBS-22 were completed during this present reporting period. NBS-22 was fabricated from single-crystal silicon, because only this material permits the required degree of fabrication precision. The test pattern consists of four solar cells, each surrounded by arrays of microelectronic test structures from which various cell and material properties and parameters can be determined. In each array, test structures to measure emitter and metallization sheet resistance, metal-to-emitter contact resistance, substrate resistivity, and carrier density in the base as a function of distance below the metallurgical junction are included. One of the solar cells contains no intentional defects; one contains separations in the metallization contact to the cell of various controlled sizes; one has no separations, but does have an emitter sheet resistance which varies periodically in a stripe pattern; and one contains both separations and the emitter sheet resistance variation described above.

Development of and improvements in ancillary techniques and apparatus have continued. A new reflected-light optical system was constructed, and a simple method for aligning the reflected-light path was developed. An attachment for revealing specimen birefringence by analyzing the 1.15-μm scanning reflected light was successfully designed and tested. A substrate heater stage for heating specimens from room temperature to 160°C while they are being scanned was constructed and found to hold the desired temperature within this range to $\pm$0.5°C. Cooling stages for cooling

cells from room temperature to -20°C (thermoelectric type) and to -60°C (compressor type) were made and tested. These three items, the birefringence attachment, the heating, and the cooling stages, were constructed in anticipation of future investigations to separate various physical mechanisms which may be operative simultaneously at grain boundaries to reduce the efficiency of polycrystalline silicon solar cells.

The resolution of the scanner, both for the 0.633-μm and the 1.15-μm scanning wavelengths, was tabulated, along with the light spot deflection and the specimen working distance, for the various optical components which are on hand. This information was compiled to facilitate selection of the most appropriate optical arrangement for a given scanning assignment and to serve as a time-saving guide for others who may construct scanners based on the one developed at NBS.

The proceedings of the Workshop on Stability of (Thin Film) Solar Cells and Materials, held May 1-3 1978 at NBS, were published [1] as was a companion document "A Perspective of a Workshop on Stability of (Thin Film) Solar Cells and Materials" [2]. The Photovoltaic Material and Device Measurements Workshop (with focus on polycrystalline thin film cells) was held June 11-13, 1979 in Arlington, Virginia with 210 registrants. NBS assisted the SERI PVPO in conducting this workshop. The general purpose of the workshop was to accelerate the development of thin film cells by improving the versatility and reliability of material and device measurement techniques.

A patent application, "Nondamaging Technique for Locating Semiconductor Device Defects and Measuring Device Resistivities," D. E. Sawyer, was filed in the U.S. Patent and Trademark Office by the DoE on May 25, 1979.

Eighteen visits to NBS were made by PVPO, industry, or academic staff during the year to discuss various aspects of the laser scanner to measure experimental solar cells whose development is being supported by PVPO.

The publications and patent applications associated with the work conducted in this reporting period are listed in Appendix A.

2. APPLICATION OF THE LASER FLYING-SPOT SCANNER TO SOLAR CELLS AND MATERIALS

2.1 Overview

During this reporting period, the scanner was used to investigate samples of both conventional single-crystal silicon p-n junction solar cells and cells or prototypes constructed using either less well-developed semiconductor materials or exploratory device concepts. From the latter group, four examples of cells or cell concepts have been selected for discussion. This is because the results obtained should be of interest to the main readership

of this report: those members of the photovoltaic community working with newer materials or exploratory device concepts. Scanning of the cells and prototypes discussed in this section was performed with the suppliers present to assist in the rapid transfer of the scanning results and effective dissemination of the scanning techniques used.

2.2 Experimental Zinc Phosphide Schottky Diodes

Measurements were made on a Zn_3P_2 Schottky diode specimen provided by the Institute of Energy Conversion (IEC) at the University of Delaware. The purpose of the measurements was to assess the spatial uniformity of the minority carrier diffusion length. The Zn_3P_2 specimen was p-type with a carrier concentration of about 10^{16} cm^{-3}.

An opaque layer of magnesium was deposited by the IEC to form Schottky barriers in the form of two semicircular patterns as illustrated in figure 1; their 3-mm diameters were separated by about 0.2 mm. Specimens prepared in this form have been used by the IEC in their work using two experimental procedures for determining the effective minority carrier diffusion length in Zn_3P_2 through spectral response measurements [3]. A third and simpler method used by the IEC to determine the diffusion length employs a focused light spot. By moving the specimen with a micrometer stage and measuring the short-circuit photocurrent as a function of the distance of the light spot from the edges of the diameters of the opaque Schottky barrier patterns, an effective minority carrier diffusion length can be obtained. This method gives results which are in good agreement with the other two [4]. However, the focused light-spot technique is tedious and time-consuming since the specimen is moved manually under the light spot, particularly so when one wishes to compare diffusion lengths for several specimen locations.

The work performed at NBS with IEC personnel on one of their Schottky barrier specimens showed that an assessment of diffusion length uniformity can be made in a straightforward and rapid manner using the laser scanner. Scanning was performed using 0.633-μm laser light. The photoresponse maps obtained by photographing the display screen were subsequently interpreted by the IEC as showing that a good degree of spatial uniformity was exhibited for the minority carrier diffusion length. They also interpreted these results to obtain a mean value which was in satisfactory agreement with that previously obtained using the more tedious fixed-light-spot traveling-specimen method.

2.3 Silicon Tandem Junction Cells

Tandem Junction Cells (TJC) provided by Texas Instruments Inc. were scanned. The design of these devices is novel in that the cell has junctions on both the illuminated and nonilluminated faces, but the junction on the illuminated face is left to "float" electrically; contacts are made only to the nonilluminated (back) face [5]. This permits all of the top cell surface to be used for photovoltaic conversion, and it also allows a great deal of flexibility in connecting cells into modules. A sketch of a TJC is shown in figure 2. The cell is modeled as a phototransistor, and ultimate AM1 efficiencies of 20 percent or better are anticipated [5].

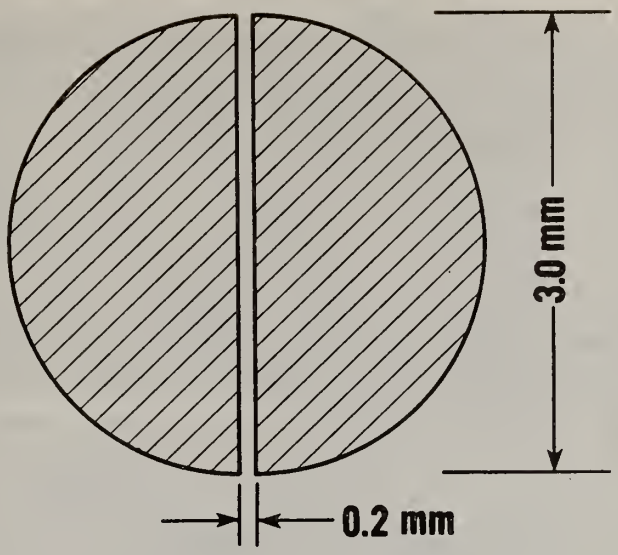

Figure 1. Sketch of semicircular magnesium metallization contact patterns deposited to form Schottky barriers on p-type Zn_3P_2.

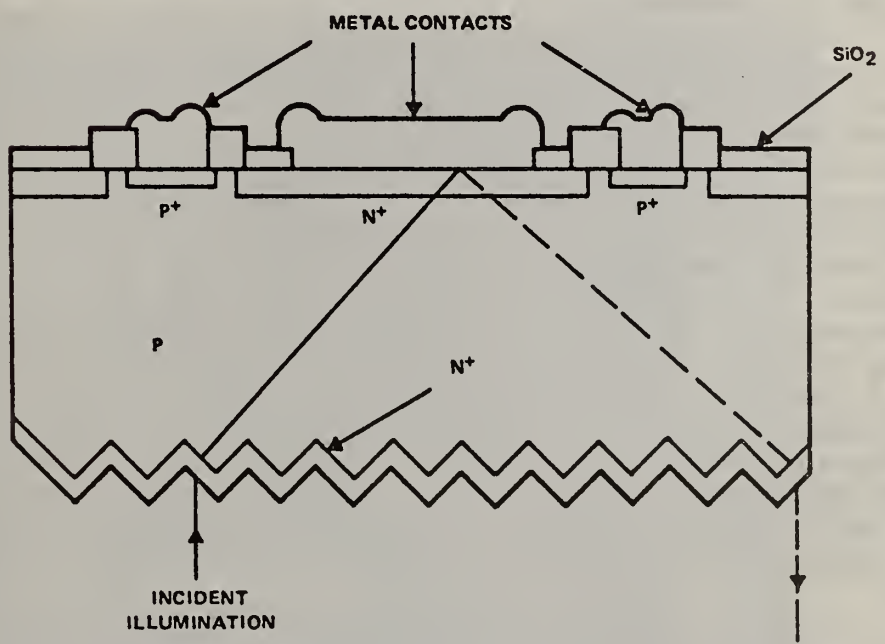

Figure 2. Sketch of a tandem junction solar cell. The light path is shown striking the back surface at greater than the critical angle of 15 deg to reflect along the path of the dashed line.

Scanning was performed on typical TJCs with the cells unbiased using both 0.633- and 1.15-μm laser light. Decreases in the photoresponse to 0.633-μm light over the p^+ base and to 1.15-μm light over both the p^+ base and the n^+ collector metallization were detected. These observations led to several speculative interpretations that suggested design modifications that could increase the overall efficiency of these cells [5].

An expression of the value of the scanner is contained in the following quotation [5]:

> "This very preliminary work indicates the potential power of laser scanning as a diagnostic tool. Further development of the technique and of the data interpretation could be very beneficial in the development of high efficiency solar cells."

2.4 Ungridded Cu_2S/CdS Cells

Scanning of a Cu_2S/CdS cell prior to gridding showed that it is possible to screen cells for quality before the most expensive fabrication step, gridding, is undertaken. Additionally, the need for careful handling of cells during fabrication was underscored by making measurements on the ungridded cell before and after scratching a cell as might occur during careless handling or by the use of improper tools. The cell scanned was made by the IEC using their current standard process. Cells of this type are fabricated on 2 by 2 cm thin copper sheets which serve as the back contact to the cell. It was anticipated by the IEC that a temporary, yet satisfactory, contact to the top side of the junction could be made with copper-coated brass clips contacting edges of the cell, provided that the cell was properly biased for the assessment.

Figure 3 shows the response for the ungridded cell using 0.633-μm scanning light and before the cell was scratched. The top side was contacted as described above. The cell was reverse biased 0.6 V. Reverse-biasing greatly reduces the cell distributed shunt conductance, a conductance inherent in the voltage-current nature of the cell. With the conductance reduced, collection of photocurrent becomes relatively insensitive to the resistance of the emitter between the point of photoexcitation and the top collecting electrode. This means that an assessment of the photocurrent produced anywhere over the cell area can be made without taking steps (by, e.g., gridding the cell) to ensure a low-resistance emitter current path. In figure 3, the vertical deflection of a scan line at a given point is proportional to the photocurrent produced by the cell. The overall photoresponse is quite similar to that observed when scanning gridded Cu_2S/CdS cells except, of course, there are no grids in the present case to shadow the cell from the scanning light spot. The depressions in the picture at the bottom, and at the upper left, are due to shadowing by the contact clips.

Figure 4 shows the response for the same cell and operating conditions after dragging one tip of a pair of steel tweezers across the cell surface. The effect of this localized damage can be seen by the lowered photoresponse in the scratched region about one-third the way down from the top of the figure. Plastic tweezers are recommended by the IEC for cell handling, but sometimes

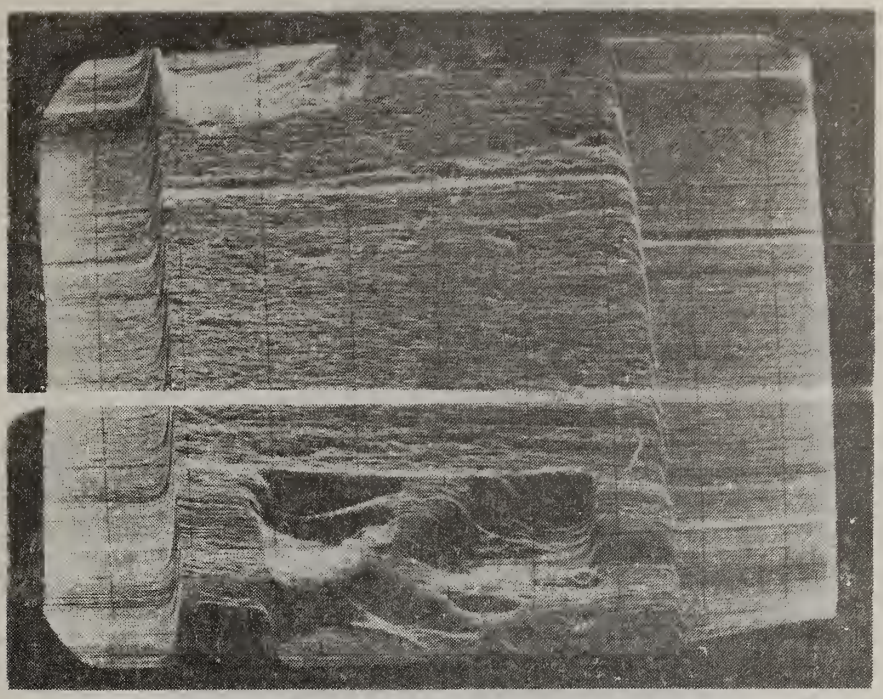

Figure 3. Ungridded Cu_2S/CdS cell response to 0.633-μm scanning light.

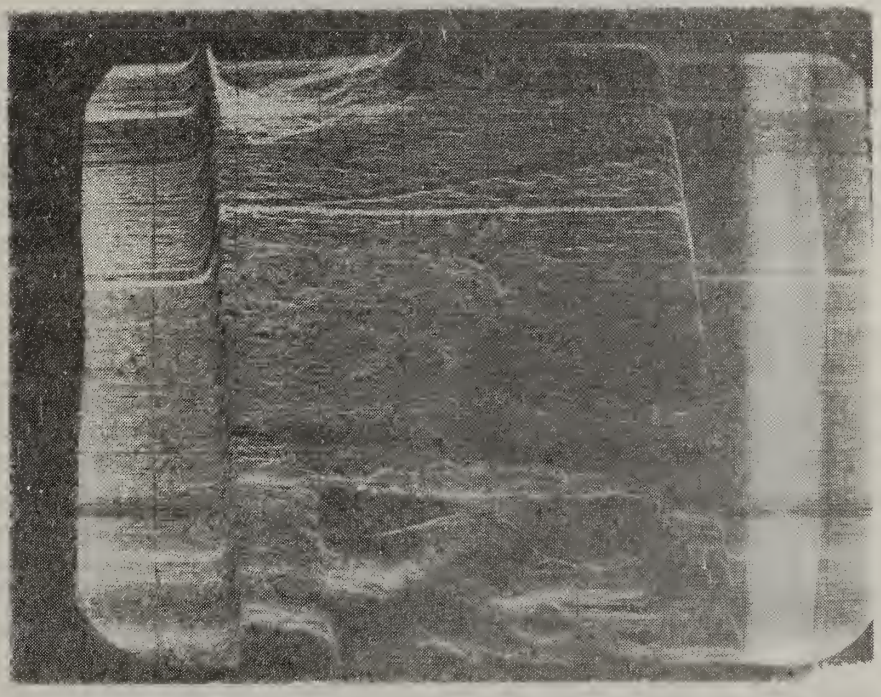

Figure 4. Ungridded Cu_2S/CdS cell response after scratching the surface.

steel tweezers are inadvertently used by the production line workers. Comparison of figures 3 and 4 underscores the need to maintain proper handling techniques.

2.5 EFG Polycrystalline Silicon Cells*

2.5.1 Defect Location

A study of EFG (Edge Fed Growth) thin film silicon solar cells was made on cells furnished by the Mobil-Tyco Solar Corporation. This work is reported in somewhat greater detail than other visits as an example of the productive collaboration that can occur with industry in the use of the scanner and in recognition of the excellent work of Dr. Yates.

Raster scans were first made to identify regions in solar cells where various types of defects were seen to occur. Line scans were then made through these regions of interest to make a more quantitative analysis of the defects. For example, figure 5 is the photoresponse map of an early low-cost n-on-p EFG cell scanned using 0.633-μm light while forward-biased at 500 mA using an external current source. The display mode used was intensity-modulation of the cathode ray beam with the "grey scale" reversed from that conventionally used; i.e., in figure 5 the darker regions correspond to regions of greater signal collection. Some cell features are readily identifiable; the white patch above finger 1 coincides with missing antireflection coating. This was established by visual inspection, and confirmed by the fact that the decrease in signal response occurs for both "bias off" and "bias on" scanning conditions to rule out conduction defects. A break is shown in finger 2; lighter areas such as the region to the left of this break indicate reduced current collection. Breaks also occur in fingers 3, 4, 5, 7, 8, etc. The white dots above finger 11 are due to the presence of silicon carbide particles; their "signatures" are apparently much larger than the actual particle sizes which may indicate low minority carrier lifetime near the particles due to surrounding impurities or defects. Alternatively, the particles may cause localized junction shunting. The calculations of Lehovec and Fedotowsky [6] also show that the photoresponse in the vicinity of localized shunts should decrease as the scanning light spot approaches the shunts.

2.5.2 Silicon Carbide Particles

The presence of silicon carbide particles is a common problem when graphite crucibles are used to contain the molten silicon in EFG techniques. Some insight into the way these particles affect cell performance may be obtained by comparing the photoresponse shown in figure 6 to that predicted by Lehovec for a point shunt, as seen in figure 7, where the effect of the point shunt is shown by the dotted lines. The reduced photoresponse as the laser spot approaches the particle is thus the signature of a point shunt. The difference between a shunting and a nonshunting silicon carbide particle,

---

* The work reported in this section was performed at NBS by Dr. D. A. Yates of the Mobil-Tyco Solar Energy Corporation with the cooperation of NBS. It was abstracted from Mobil-Tyco trip reports and edited, and appears with the permission of the Corporation.

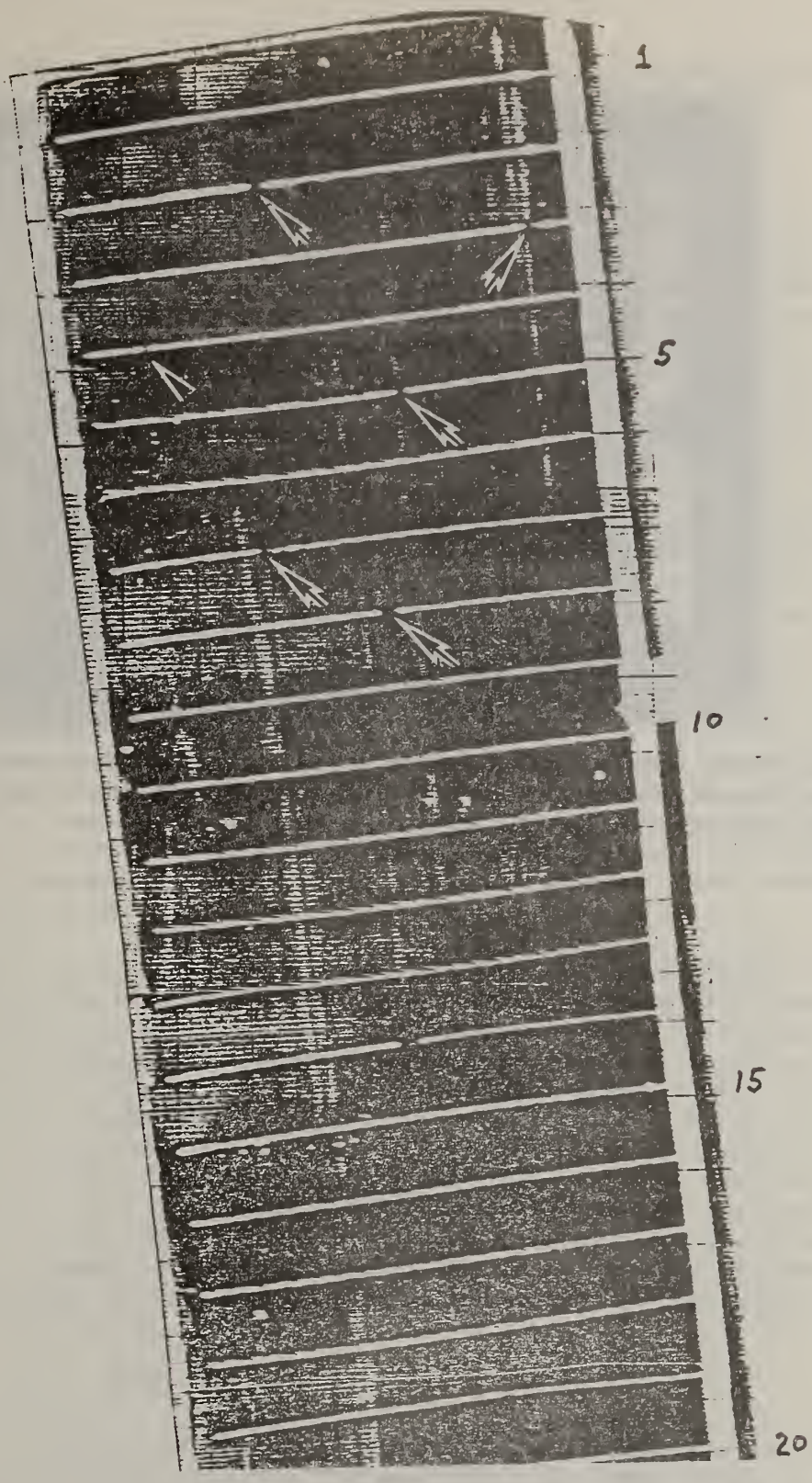

Figure 5. Photoresponse map to 0.633-μm light of an early low-cost EFG cell with 500-mA forward bias. Breaks in metallization mentioned in text are indicated with arrows.

Figure 6. Photoresponse of an EFG cell near a silicon carbide particle producing a point shunt through the cell indicated by the reduced signal as the laser spot approaches the particle.

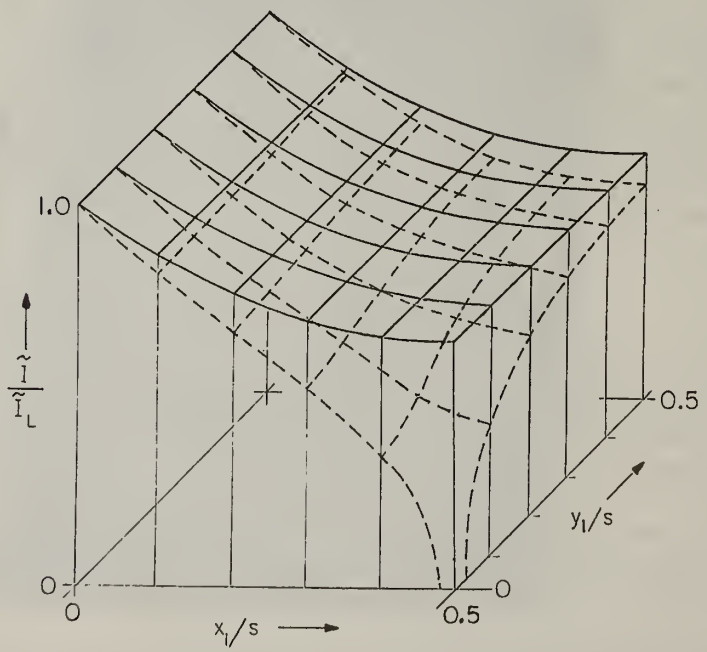

Figure 7. Predicted photoresponse of a cell with a point shunt located at 0.5 (dotted lines) compared to a perfect cell (solid lines).

which shadows the junction, is shown in the line scan in figures 8 and 9, respectively.

2.5.3 Crack Parallel to a Metallization Finger

The detection of cracks in forward-biased single crystal silicon cells with a laser scanner was previously reported by NBS [7]. Figures 10 and 11 show that cracks may also be found in EFG cells and detected using the same scanning technique. The cell scanned is 2 cm by 2 cm and was fabricated under DoE sponsorship. Figure 10 is the 0.633-μm photoresponse for a steady-state irradiance of a few suns and with the cell dc open-circuited. The grey scale is reversed from that used for figure 5; i.e., regions of greater photoresponse now appear lighter. There appears to be a linear defect (as indicated by a dark line) between the second and third fingers from the left. Figure 11 is a line scan through the defect region. The photoresponse is discontinuous across the defect; also, the photoresponse at the two edges of the defect is such that the edge closer to a metallization finger provides the greater photoresponse. This behavior is predicted for a cracked cell by Lehovec and Fedotowsky's analysis [6]. Use of an optical microscope confirmed that the cell indeed was cracked in the region indicated by the scanner display. The nonzero photoresponse slope at the crack edges indicates either ohmic shunting across, or minority carrier recombination at, the cracking boundary, or a combination of these two. It is possible that the contributions from these two mechanisms may be separated through the use of ancillary measurements. The shunting contribution might be computed from a measurement of temperature rise at the crack for a given value of cell reverse bias. Localized temperatures can be measured using commercially available microradiometers, or by using a thermal phosphor sheet pressed against the cell surface [8].

Further studies of the cell with a crack parallel to a metallization finger were made which showed the difference between the signature of a crack in the active cell region and one in which the crack also extends to the bus bar metallization. The same cell as used for figures 10 and 11 is shown in figures 12 and 13 in a scan over only the cracked region. Figure 12 shows the characteristic photoresponse signature as predicted by theory [6] for high electrical resistance across the crack. At a later time when the crack had spread to partially interrupt the bus bar, the effect is seen as a lower photoresponse even near the right-hand finger as compared to the left-hand side, figure 13. The extent of the reduction of current collected past the partial break is shown in the line scan in figure 14 directly adjacent to the bus bar. Only about three-fifths of the normal current is collected from the right side of the crack.

2.5.4 Back Contact Faults

Figures 15, 16, and 17 are scanner display photographs near the end of a 1-cm by 4-cm high-quality (11 percent efficient) EFG cell. Figures 15 and 16 are for 0.633-μm laser light scanning. The cell is unbiased in figure 15 and under a light bias of about 3 suns for figure 16. Figure 17 is for 1.15-μm scanning with the cell unbiased. The causes of some of the "features" which appear in both figures 15 and 17 and are enhanced with irradiance (fig. 16) are presently not explained. Microscope observations did not reveal cracks,

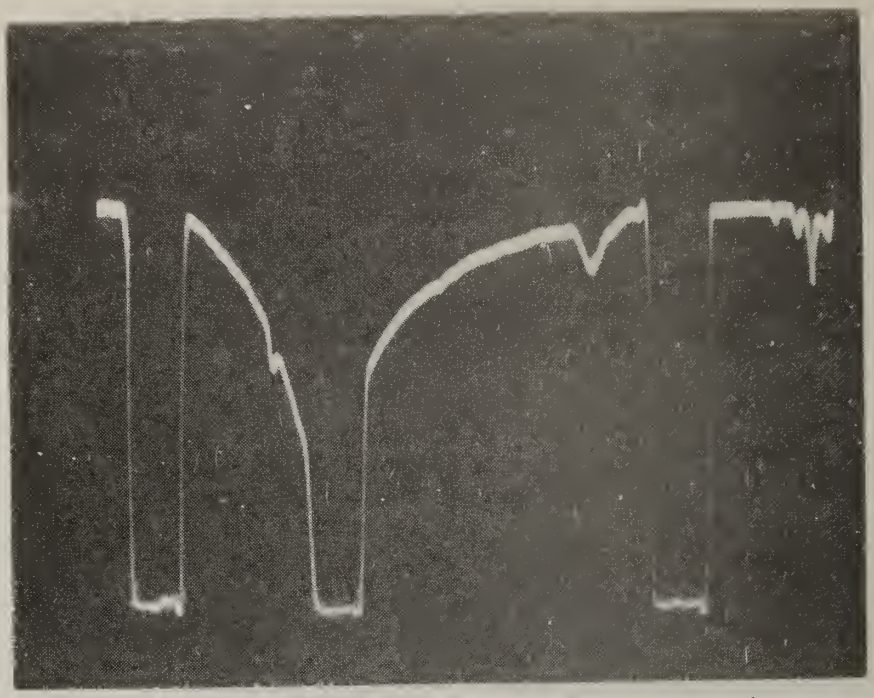

Figure 8. Line scan through the region of a cell where a silicon carbide particle is producing a point shunt.

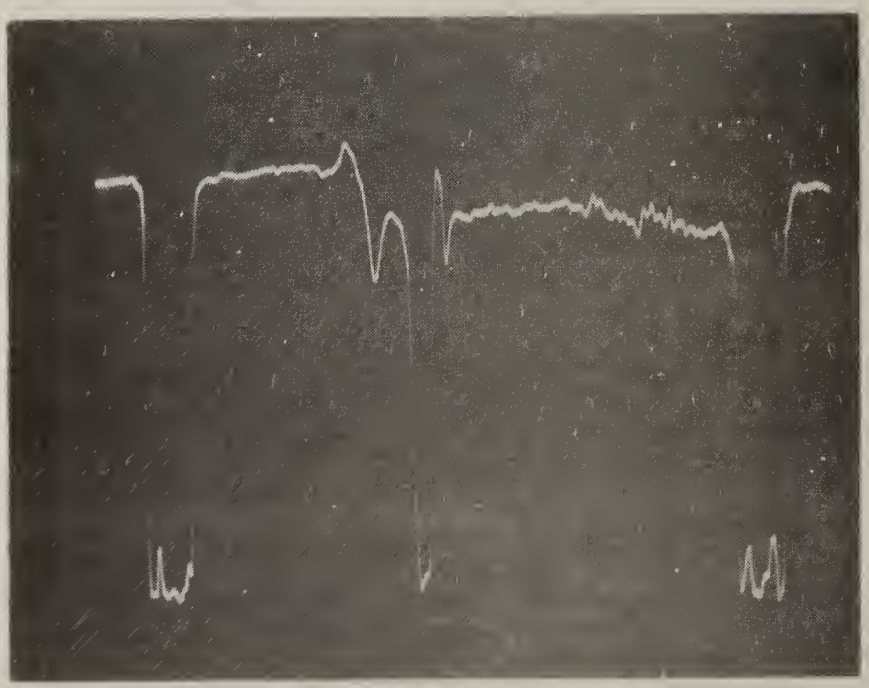

Figure 9. Line scan in the region of a cell when a silicon carbide particle has not produced a shunt through the cell.

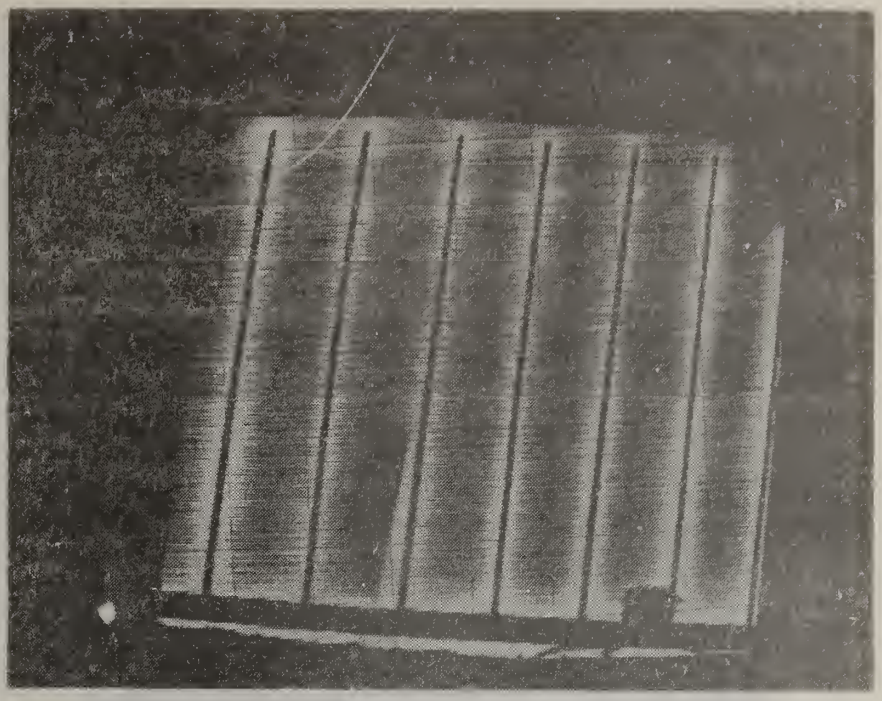

Figure 10. Raster scan of an EFG cell under a few suns light bias to identify a hairline crack between the second and third metallization finger from the left.

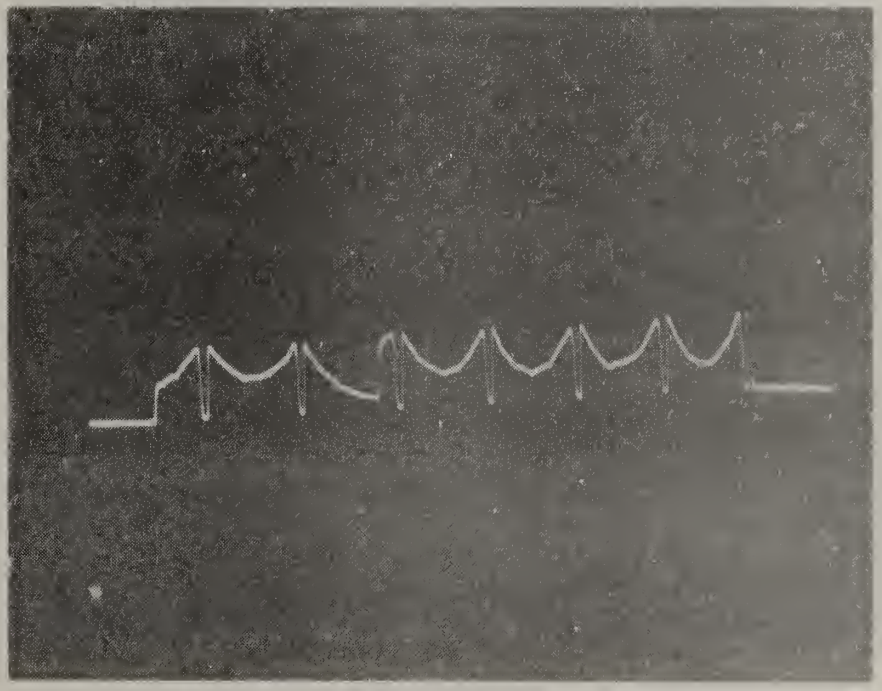

Figure 11. Line scan of the cracked region of the cell in figure 10.

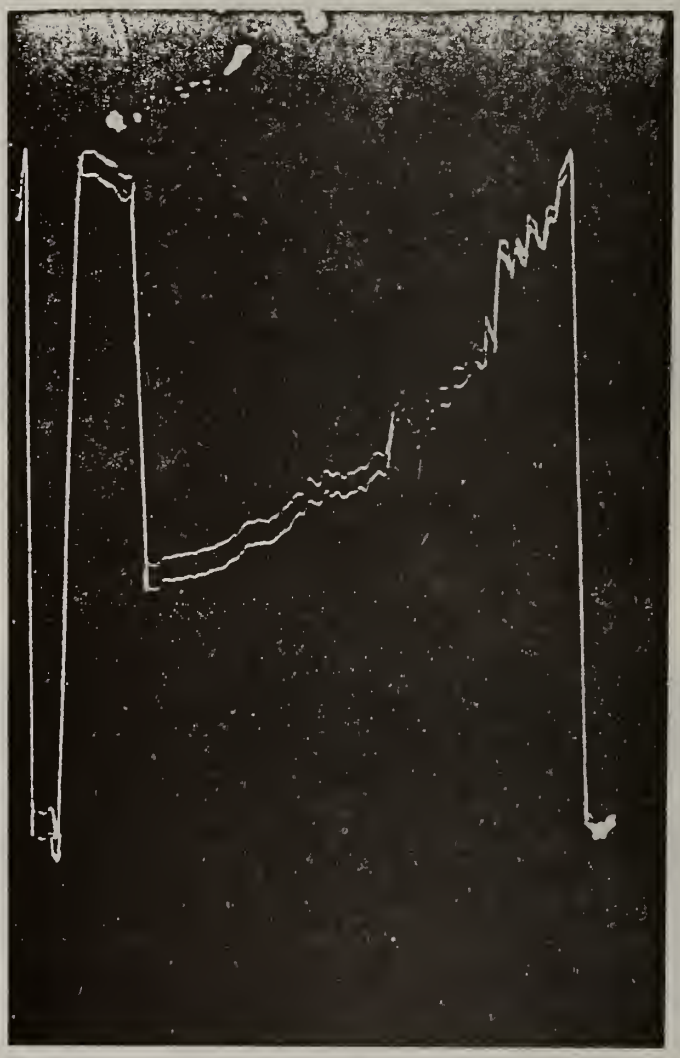

Figure 12. Expanded line scan of the previous cell before the crack has spread to the bus bar metallization. Direction of scan on cell is opposite to that for the one used in figure 11.

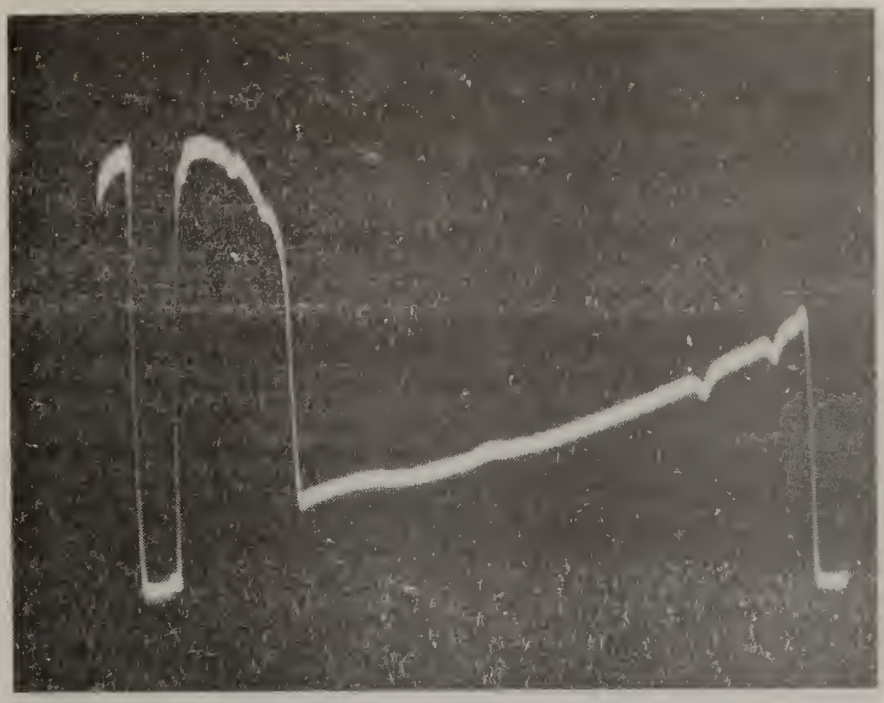

Figure 13. Same cell as in figure 12 at a later time when the crack has interrupted the flow of current along the bus bar. Note the lowered response all the way to the right-hand grid.

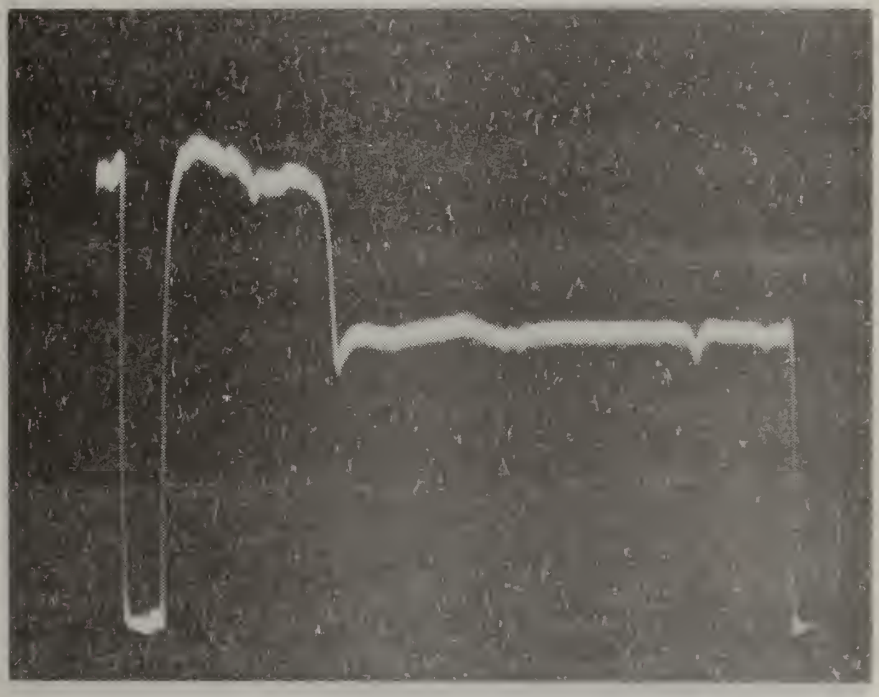

Figure 14. Line scan adjacent to the bus bar showing the reduction in photoresponse due to the crack.

Figure 15. Photoresponse of a high quality 1-cm by 4-cm EFG cell. Laser light is 0.63 μm with no light bias.

Figure 16. Cell of figure 15 under about 3 suns light bias.

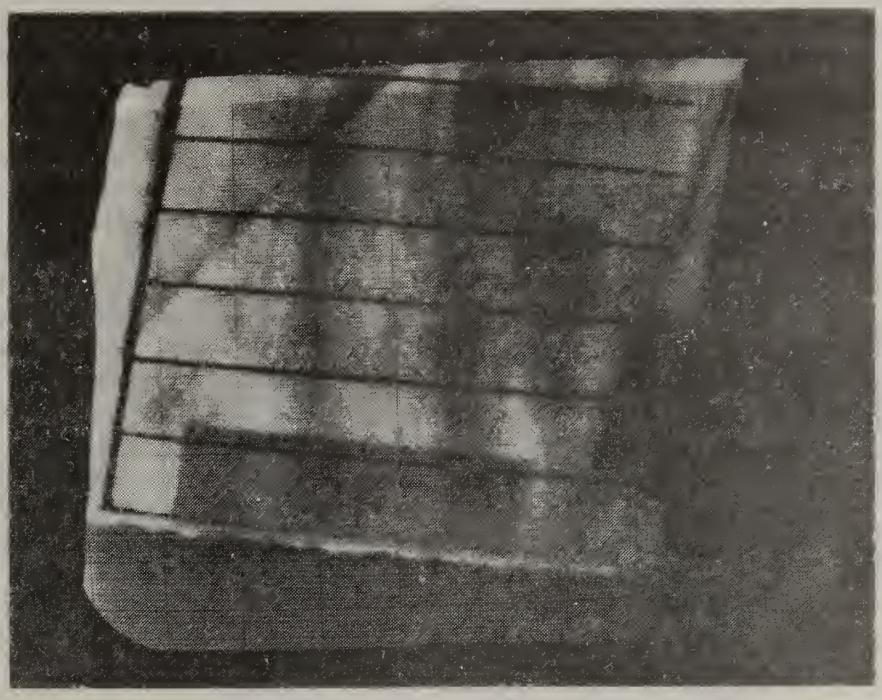

Figure 17. Cell of figure 15 under no light bias but with 1.15-μm laser light indicating the photoresponse at the back contact more clearly.

but cracks cannot be ruled out. These features include the lowered photoresponse of the far-right cell portion between fingers 1 and 6 (counting from the top), and the diagonal line between fingers 1 and 4. The use of 1.15-μm scanning light (fig. 17) enhanced these features and added a few more such as the diffuse patterns near the center. The very regular shape of the rectangular patch overlapping fingers 6 and 7 in figure 17 argues against its being due to a crystal defect. The same region exhibited a reduced 0.633-μm photoresponse with 3 suns background (fig. 16), indicating a conduction defect. Taken together, these two observations suggest that the patch in question originated during cell fabrication. Cells are fabricated from p-type EFG sheets by first diffusing a n^+ skin to form the n^+p photojunction. This diffusion creates an n^+p junction in the back side as well. Tabs are used to support the ends of the diffused wafers during evaporation of aluminum onto the back side. The wafer is then heated in vacuum to alloy the aluminum through the back side n^+ skin and to make ohmic content with the p-type base. The specimen is then placed in another fixture (which supports the specimen by its edges), and a trimetal mixture of chromium, titanium and silver is deposited over the aluminum for protection against corrosion. The rectangular patch visible in figure 17 matches the geometry of the end tab used to hold the wafer during aluminum evaporation. Because this tab masks a portion of the specimen against the aluminum evaporation, the n^+p barrier beneath it remains intact. This creates a high-resistance base contact region and explains the lowered photoresponse of the forward-biased cell between fingers 6 and 7 in figure 16. The interpretation of the enhanced 1.15-μm photoresponse which allows a "shadow" of the tab to be visible in figure 17 is that the reflection of 1.15-μm light is greater from the p-base, aluminum interface than it is from the multilayer consisting of the p-base, n^+ skin, and trimetal composition. A greater reflection allows more of the 1.15-μm light (which is but weakly absorbed within the silicon) to make a second pass through the photosensitive junction region and add to the cell photoresponse. It is noteworthy that, to the eye, all portions of the back contact appeared to be the same. The missing aluminum was masked from observation by the trimetal film.

2.5.5 Deliberate Scratches

To study the effect of surface scratches on the photoresponse, deliberate scratches were made with a diamond scribe before the plating step. If the scratch caused an ohmic shunt, reduced photoresponse should be observed as the laser spot approaches the scratch. This was not observed and subsequent Liquid Crystal Thermography using reverse bias on the cell confirmed that there was no evidence of high leakage current at the scratch site. This suggests that the laser scanner can differentiate between serious deep cell scratches and relatively harmless shallow ones.

2.6 New Applications

Two new areas in which the laser scanner may be able to provide important measurements of solar cell operating characteristics were identified during the contract period. One is a test of bandgap narrowing as a function of dopant density. This is an area of considerable current theoretical activity [9-11] and one in which careful experimental work is needed. The contribution of the electron-hole pair separation energy to the bandgap was

calculated by H. P. D. Lanyon as a function of dopant density and temperature [9]. To check the temperature dependence, cooling stages were designed and built as described in sections 5.5.2 and 5.5.3. Preliminary measurements of the change in photoresponse over a range of 23°C to -60°C gave the expected reduction in photoresponse with lower temperature for dopant densities measured. However, additional work is needed to establish a quantitative dependence of this change on dopant density.

The second new area is an attempt to separate the resistive effects that limit the current collected in a solar cell from those due to recombination in the cell. A suggestion was made by the principal investigator (D. E. Sawyer) to attack this task by measuring the photoresponse of a forward-biased test cell with the laser scanner and then using an infrared detection system to map the recombination radiation in the same cell area and for the same value of forward-bias current. This idea was stimulated by G. W. Turner's paper at the Photovoltaic Material and Device Measurements Workshop [12].

3. MATHEMATICAL MODELING

A report on the initial modeling work performed by Drs. Kurt Lehovec and Andre Fedotowsky of the University of Southern California under subcontract has been published [6]. It extends the work previously performed by them on the analysis of laser scanning techniques applied to solar cells. Work previously reported [7] developed the basic equations and applied them to fault-free cells scanned either by a line-shaped light beam or a focused spot and showed that these two light geometries give the same analytical results. The report concluded with a general solution for cells having noncontacting electrode sections. During the present reporting period the equivalency of line and spot scanning, for all cells including those with defects, was proven, and results for the following were obtained: cells containing point shorts and cells cracked both parallel to the metallization fingers and at various angles to these fingers, and with various values of crack shunt conductance. The complete report is published separately [13].

4. NBS-22, A SOLAR CELL TEST PATTERN

One of the needs of the laser scanning program is a means of determining the degree of agreement between cell scanning results and the results predicted analytically [6], both for "perfect" cells and for cells with various defects. To answer this need, NBS-22, a solar cell test pattern, was conceived in the first year of this program, and its final design was completed in the first half of 1979.

The NBS-22 test pattern contains four solar cell test structures which are surrounded by arrays of microelectronic test structures which can be used to measure electrically various solar cell and material parameters. One cell is perfect and the other three have combinations of process variations including regions where the metal does not contact the silicon and regions with different sheet resistance. The arrays of microelectronic test structures include van der Pauw cross-sheet resistors [14], a contact resistor [15], a four-probe resistor [16], an MOS capacitor [17], a dc MOSFET dopant profiler [18], and a junction diode [19]. These structures can be used to

determine sheet resistance, contact resistance, substrate resistivity, dopant profiles, and defect recombination centers. It has been demonstrated [20] that these measurements and others can aid in the control of a semiconductor fabrication process. With the microelectronic test structures deployed around each of the four solar cells, not only may "spot" values of the quantities of interest be obtained, but their variation over the wafer may also be inferred. The sheet resistance determined by electrical measurements may be compared with independent measurements made with the laser scanner. A measure of the contact resistance, also obtained by electrical measurements, served to check the quality of the metallization contacts to both the solar cells and the test structures. The remaining structures were included for possible use in connection with future studies of solar cell measurement techniques.

Initially, efforts to fabricate the photomasks needed to produce the test pattern encountered problems due to the requirement that the computer-controlled pattern generator work both with the very small microelectronic test structures and with the much larger solar cells. These problems were surmounted, and satisfactory photomasks and wafers containing the test pattern were fabricated during this reporting period.

4.1 Description of the Pattern

The solar cell test pattern, NBS-22, is illustrated in figure 18, and the solar cell test structures, which are approximately 1 cm on a side, are labeled A, B, C, and D. Surrounding these cells are the arrays of microelectronic test structures which are 2.44 by 1.60 mm on a side. The arrays have a step-and-repeat distance of 2.540 mm in both the x- and the y-directions. In the actual test pattern, no array occurs in the rectangles shown in the figure which contain either a diagram of the array or an "x."

To fabricate the test pattern, four photomasks are required: level 1 delineates the doped regions; level 2, the oxide contact openings; and level 3, the metal probe pads and metal interconnects. To alter the emitter sheet resistance systematically, there is a fourth mask, level 4, used to pattern a second doped region within the area of the first. In figures 18 to 21, the contact openings are shown as cross-hatched areas, while the doped and metal regions are enclosed by solid lines. Cell A is an unaltered or "perfect" solar cell. In cell B, there are regions in the vertical fingers where contact openings are not made in the oxide resulting in no contact to the cell. As illustrated in figure 19, the "opens" in contact fingers 1 and 3 range in length by doubling from 0.25 to 16 mm, starting from the top; the pattern is reversed on fingers 5 and 7. Cell C has regular contacts as in cell A, but has alternate columns of double- and single-diffused regions to produce alternate columns of low and high sheet resistance in the emitter region. Both noncontacted regions and areas of low and high sheet resistance are included in cell D.

The pattern of microelectronic test structures which surround each solar cell is shown in figure 20. The test structures are designed with probe pads as an integral part of the structure; they are arranged in eight 2 by 10 columns, and the eight columns are separated by 300 μm. The probe pads in these columns are 80 μm on a side and they are separated by 80 μm. This

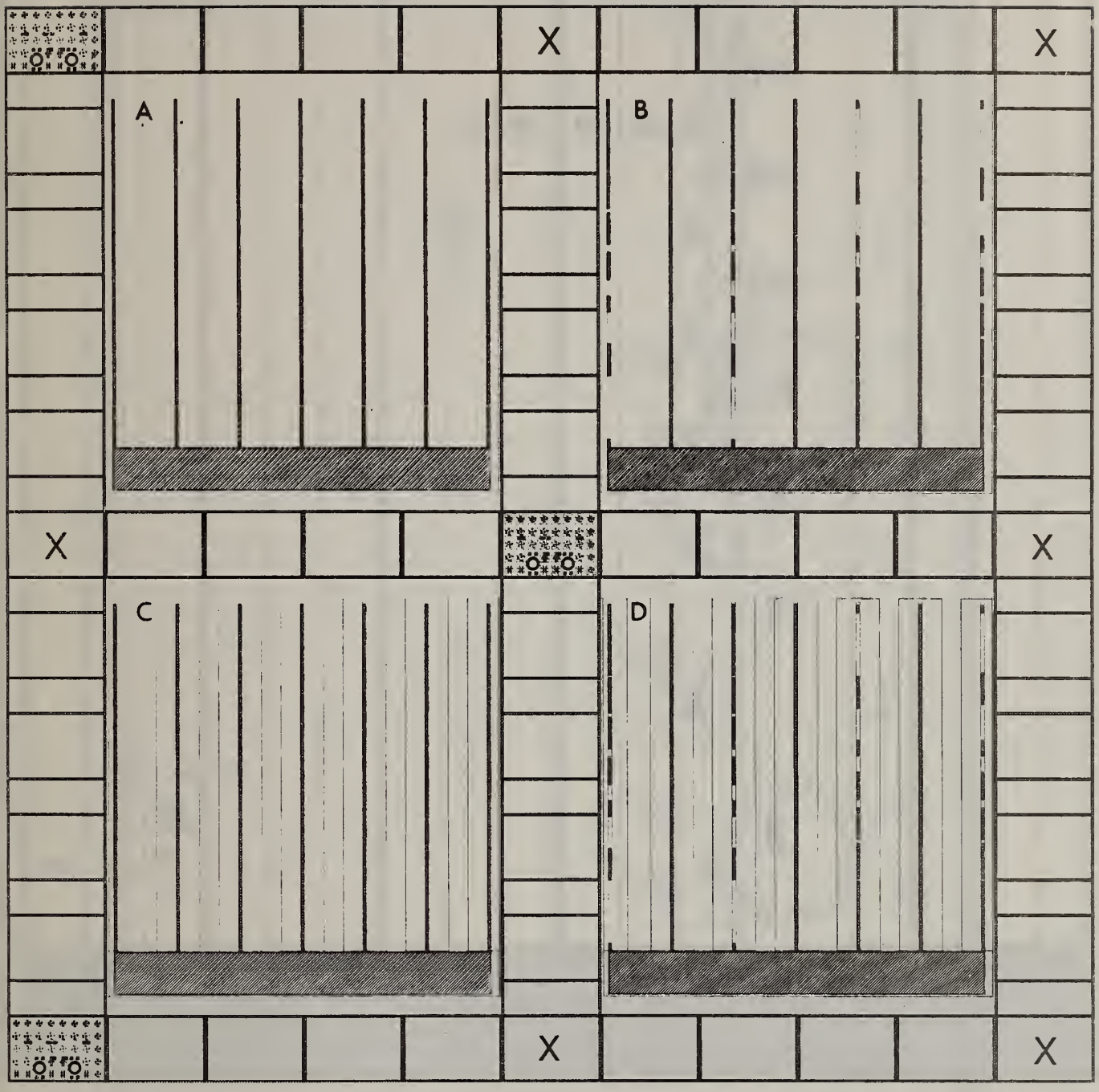

Figure 18. NBS-22 test pattern which includes four solar cells (A, B, C, and D) surrounded by arrays of microelectronic test structures. Arrays are present in every one of the larger rectangles not containing a diagram of the array or an "x".

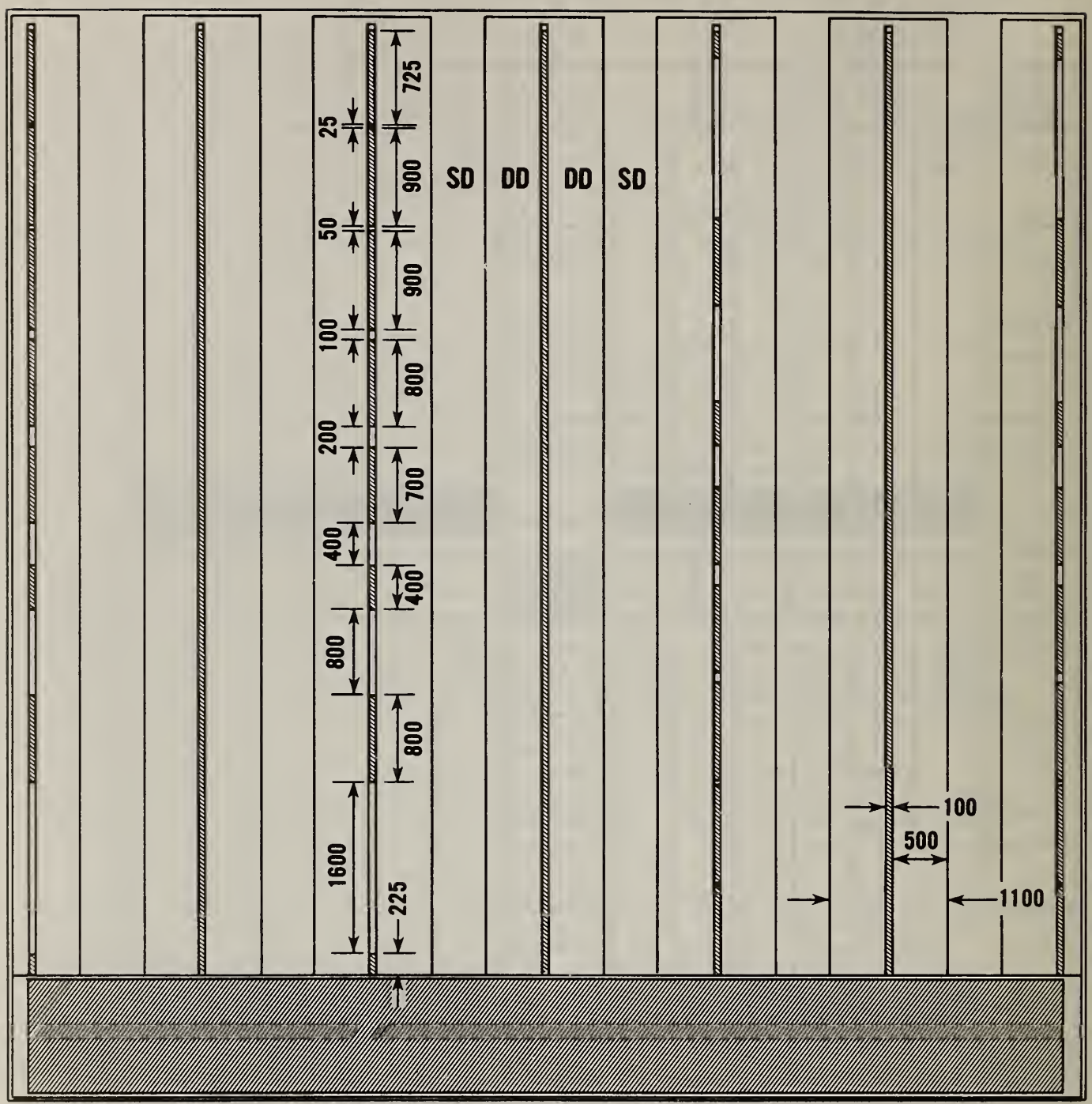

Figure 19. Expanded view of the D solar cell which contains the doubly diffused and the singly diffused regions of the cell and also the regions where the metallization does not contact the emitter surface, shown as the white breaks. The dimensions are given in micrometers.

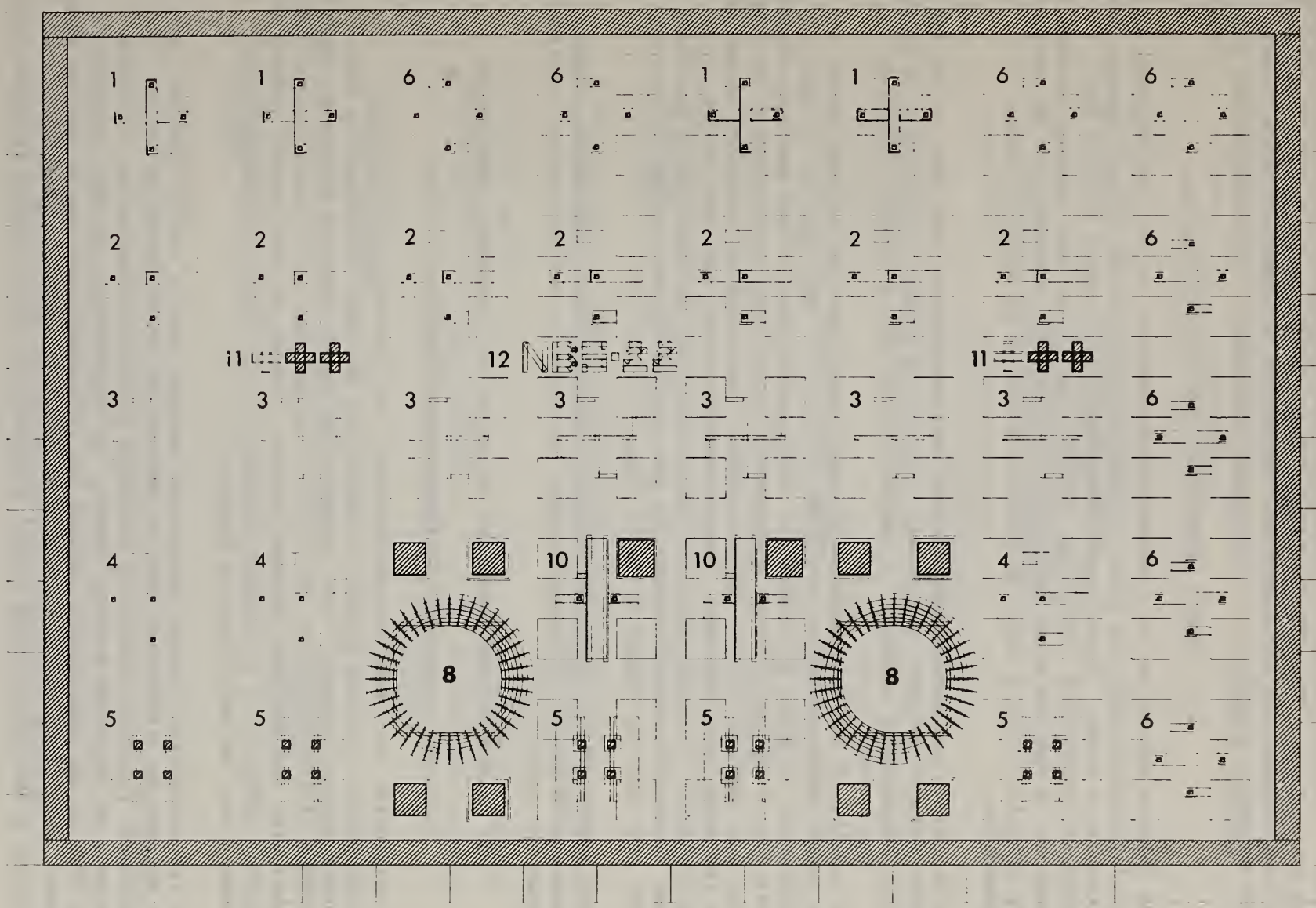

Figure 20. The microelectronic test structure pattern which surrounds the solar cell. The structures are numbered and described in table 1.

approach [21] allows automated measurements using one probe card on a wafer prober. Alternate pairs of double- and single-diffused cross test structures head the columns. The single-diffused cross structure is used to construct the last column. In the figure each structure is numbered; table 1 lists each structure together with additional information on its design and use.

4.2 Sample Preparation and Data Collection

Test pattern NBS-22 was delineated using a contact printer and conventional photolithography onto two 2-in. (51-mm) diameter *p*-type silicon wafers, one pattern to a wafer. In an inert atmosphere from a solid source, two successive phosphorus diffusions at 950°C for 15 min were used to produce the variation of emitter sheet resistance. The metal interconnects and contact pads were formed by a layer of aluminum produced by electron-beam evaporation.

The dc electrical measurements of the test structures were made on the two wafers using a computer-controlled acquisition system consisting of a wafer prober, electrical scanners, a current source, and a digital voltmeter.

The results of the measurements of sheet resistances on the two wafers for the singly diffused region are given in table 2. The location of each measurement is shown in figure 21. Each table entry is the mean and standard deviation of the set of four measurements made along the top row in each test array surrounding cell A. The mean sheet resistance and standard deviation for the whole cell indicates greater variation over the cell dimensions of approximately 1 cm than over the test arrays with an approximate dimension of 2 mm. Nominal sheet resistance for the singly diffused region is 51.5 Ω/□ while that for the doubly diffused region is 31.5 Ω/□.

Measurements of the contact-to-emitter resistance were also made. These measurements served to determine that there exists uniform contact resistance across the wafer.

5. LASER SCANNER ANCILLARY TECHNIQUE AND APPARATUS DEVELOPMENT

5.1 Improved Reflected-Light Detection System

By collecting the light reflected from a cell during scanning onto a photodetector, one may present a picture of the cell topography on the scanner display screen. This is useful by itself when one wishes to observe specimen birefringence (cf sec. 5.2). One may also mix this reflected-light signal with the specimen response signal. Mixing in this manner permits cell response features to be located accurately with respect to topographical features such as metallization fingers.

The reflected light system previously employed used a mirror inserted into the microscope illuminator port to deflect the reflected light to an "outboard" focusing lens and a germanium photodiode mounted on a bracket fastened to the laser scanner frame. One disadvantage of this arrangement was that it was difficult to shield the reflected-light system against room light. This light can be picked up by the lens or by the photodiode, and it produces a spurious display signal modulated at 120 Hz (twice the power line

Table 1. Test Structure List.

Structure Letter/Number	Test Structure Name	Specification/notes Description	Parameter Measured	Reference
A	solar cell	no process modification		-
B	solar cell	noncontacted regions		-
C	solar cell	alternate regions of high and low sheet resistance		-
D	solar cell	noncontacted regions and alternate regions of high and low sheet resistance		-
1	van der Pauw cross resistor	double-doped region	sheet resistance of double-doped region	[14]
2	contact resistor	metal-to-doped region	contact resistance	[15]
3	van der Pauw cross resistor	metal region	metal sheet resistance	[14]
4	contact resistor	metal-to-substrate	contact resistance	[15]
5	four-probe resistor	substrate	base resistivity	[16]
6	van der Pauw cross resistor	single-doped region	sheet resistance of the single-doped region	[14]
7	junction diode		recombination centers	[19]
8	MOS capacitor	field oxide over single-doped region	recombination centers, SiO_2/Si interface states	[17]
9	substrate contact			[15]
10	dc MOSFET dopant profiler	four-terminal MOSFET	substrate dopant density profile	[18]
11	mask alignment marker			-
12	NBS-22 Logo			-

Table 2. Sheet Resistance ± Standard Deviation [ohms per square].

Location, Figure	Wafer #1	Wafer #2
1	51.75 ± 0.10	49.52 ± 0.36
2	51.47 ± 0.02	48.79 ± 0.30
3	51.42 ± 0.03	48.25 ± 0.26
4	51.47 ± 0.07	47.93 ± 0.18
5	51.28 ± 0.03	47.00 ± 0.17
6	50.89 ± 0.08	46.46 ± 0.15
7	50.65 ± 0.09	46.14 ± 0.15
8	50.42 ± 0.08	45.91 ± 0.15
9	50.36 ± 0.09	46.14 ± 0.17
10	50.49 ± 0.07	46.62 ± 0.30
11	50.93 ± 0.13	47.43 ± 0.38
12	51.55 ± 0.20	48.48 ± 0.47
13	52.43 ± 0.21	50.07 ± 0.57
14	52.36 ± 0.20	50.22 ± 0.61
15	52.35 ± 0.20	50.24 ± 0.63
16	52.32 ± 0.20	50.30 ± 0.59
Mean =	51.38 ± 0.72	48.08 ± 1.61

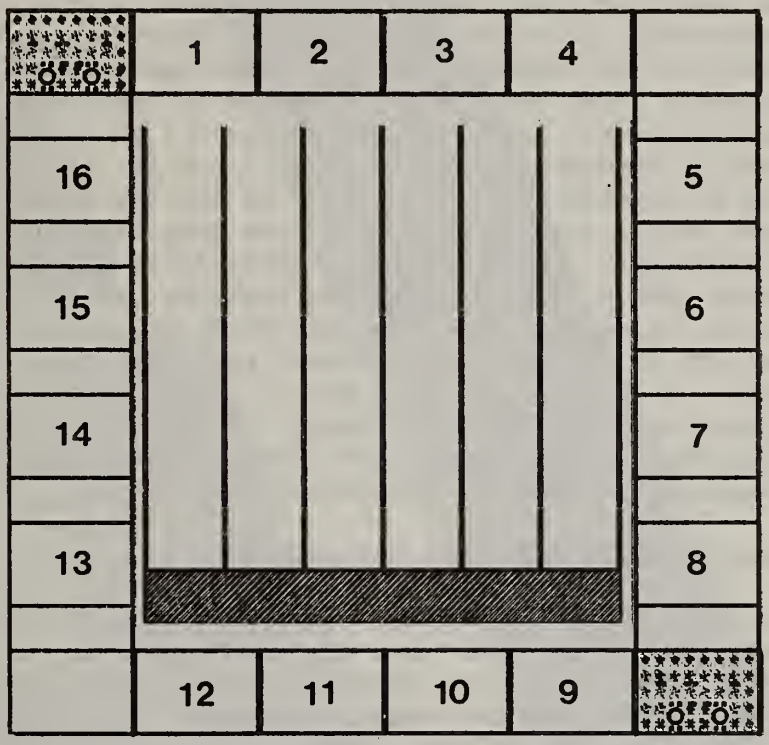

Figure 21. Sheet resistance measurement locations around cell A for values given in table 2.

frequency). A second disadvantage is that the microscope illimination port, because it was occupied by the mirror, was no longer available for other purposes. The port is actually a cylindrical tube fastened to the microscope body. It contains slots designed to hold filters for changing the spectrum of the light used to view specimens when the microscope is used in the service for which it was designed. One of these slots is needed for the rotatable analyzer used for specimen birefringence work, but it is not accessible with a mirror inserted into the illumination port.

A new reflected-light assembly was constructed to overcome the above objections. A photograph of the assembly is shown in figure 22. It screws into the illuminator port and leaves the filter slots unobstructed. The assembly incorporates a standard 10X microscope ocular, a germanium photodiode having a 3-mm diameter photosensitive surface, and a photodiode mounting arrangement which permits the diode to be readily aligned and locked in position to receive the light reflected from the scanned specimen. The alignment method is described in section 5.1.1. A few features of the assembly should be pointed out. The cutout in the barrel is used for insertion of the ocular lens and the germanium photodiode and it is normally covered with black tape. The germanium photodiode is used in the photovoltaic mode with a 10 kΩ terminating resistor, and it is wired directly to the bnc output connector. The detector socket is mounted on a circuit board which in turn is fastened to the metal rod which protrudes from the rear of the case. The rod slides in a sleeve, and the sleeve may be moved eccentrically with respect to the case axis. During alignment, the rod is locked to the sleeve by tightening a 6/32 locking screw, and the eccentric location is fixed by tightening a knurled ring.

5.1.1 Alignment of Reflected-Light Optical Path

The first step is to align the scanner mechanically so that the scanning raster for both the visible, 0.633 μm, and near-infrared, 1.15-μm, laser sources coincide. This is done by varying the mechanical adjustments for both light paths and locking the adjustments after coincidence has been achieved. A semiconductor specimen responsive to both wavelengths is used for this purpose. Coincidence of the 0.633- and 1.15-μm scanning rasters permits the near-infrared reflected light portion of the scanning system to be aligned automatically when the system is aligned visually with the 0.633-μm laser.

The reflected-light assembly, i.e., the photodetector and associated focusing lens, is removed and a reflecting pattern is fastened to the specimen rocking stage. A satisfactory reflecting pattern is provided by a fine metal-grid mesh fastened to a small, flat mirror. The particular mesh used in developing this technique was a rectangular pattern with a series of 25-μm wide bars with a 375-μm separation. The 0.633-μm (visible) laser is selected, and the scanning mirrors are energized. A white card or a piece of frosted glass is positioned in the (unfocused) reflected light beam, and the rocking stage micrometer heads are adjusted so that the amount of light scattered from the card, observed visually, is maximized. The card is then removed and the reflected light assembly put back in place. The detector portion of the assembly is designed so that the detector may be moved axially with respect to the lens, and eccentrically with respect to the optical axis of

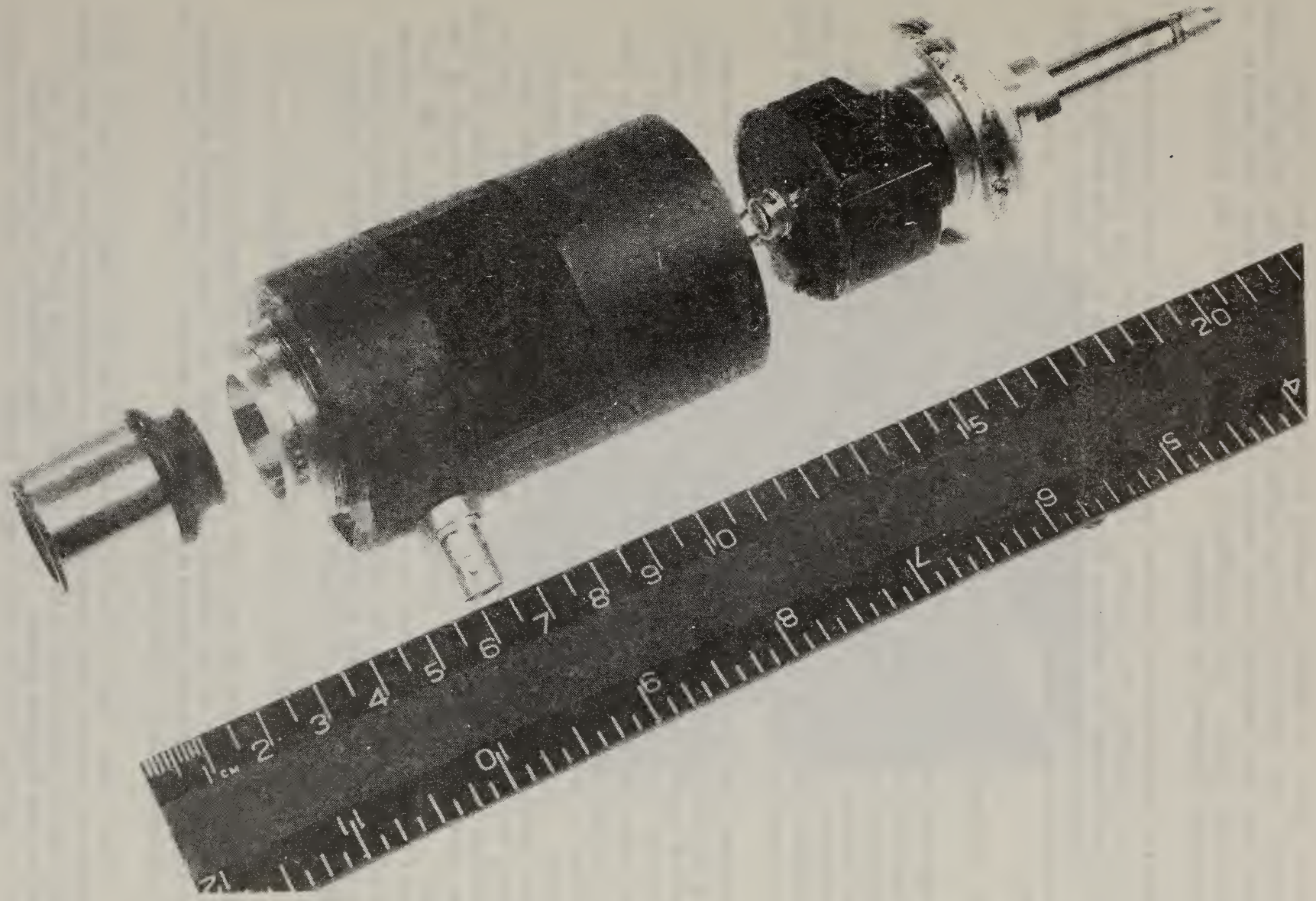

Figure 22. New reflected-light assembly using a germanium photodiode visible on the right-hand component.

the lens. With the detector serving as the input to the scanner display electronics, the detector is moved eccentrically to place the reflected-light image of the grid pattern in the center of the display screen, and axially to maximize the signal. Both adjustments are then locked and the reflected-light system alignment is complete.

The desired semiconductor specimen can now be fastened to the rocking stage. Because the incident and reflected-light paths are both now properly aligned, the only mechanical adjustments that have to be made to obtain reflected-light information are the rocking stage micrometer heads. These are adjusted for a maximum specimen reflected-light signal using the desired laser source.

5.1.2 Photomultiplier Detector

The improved reflected-light detection system described in the previous section still suffers from the rather limited area of the specimen that can be displayed with the reflected light. The reason for this is that the system depends on the light reflected from the specimen being intercepted by the objective of the microscope. When areas larger than about 1 mm on a side are scanned, the angle of incidence of the laser beam on the specimen is such that no practical lens can intercept the reflected light.

To overcome this limitation, another approach was explored. This approach uses a partially reflecting mirror under the objective lens to deflect the reflected light to an appropriate detector. The flexibility in the location and area of the mirror allows the interception of reflected light from a larger area than before. The exploratory effort described here used a thin glass microscope slide for the mirror and a photomultiplier, with an S-1 response, to monitor the light reflected from the glass slide as shown in figure 23. A neutral density filter with a transmission of approximately 1 percent, placed in front of the photomultiplier, was used to reduce light reaching the cell from the sample. While no effort was made to optimize the system and to determine scanning area limits for the approach, areas as large as one centimeter on a side could be displayed in the reflection mode of the scanner. The uniformity of the response of the photomultiplier of its face was sufficiently uniform that no optical focusing of the reflected light was necessary in this exploratory effort. An example of the response obtained using this reflective mode to scan the surface of a solar cell A on Test Pattern NBS-22 is shown in figure 24.

5.2 Specimen Birefringence Microscope Attachment

The general usefulness of the laser scanner for investigating semiconductor interface phenomena in polycrystalline silicon cells was enhanced by adding a birefringence detection capability to the reflected-light optical circuit for the plane-polarized 1.15-μm scanning laser.

The 1.15-μm laser light is weakly absorbed in single crystal silicon at room temperature. Much of the scanning light can be reflected from the cell back-contact metallization and collected by the reflected light detection and imaged on the display screen. Of course, light directly reflected from surface features, such as metallization fingers is also imaged. Additionally,

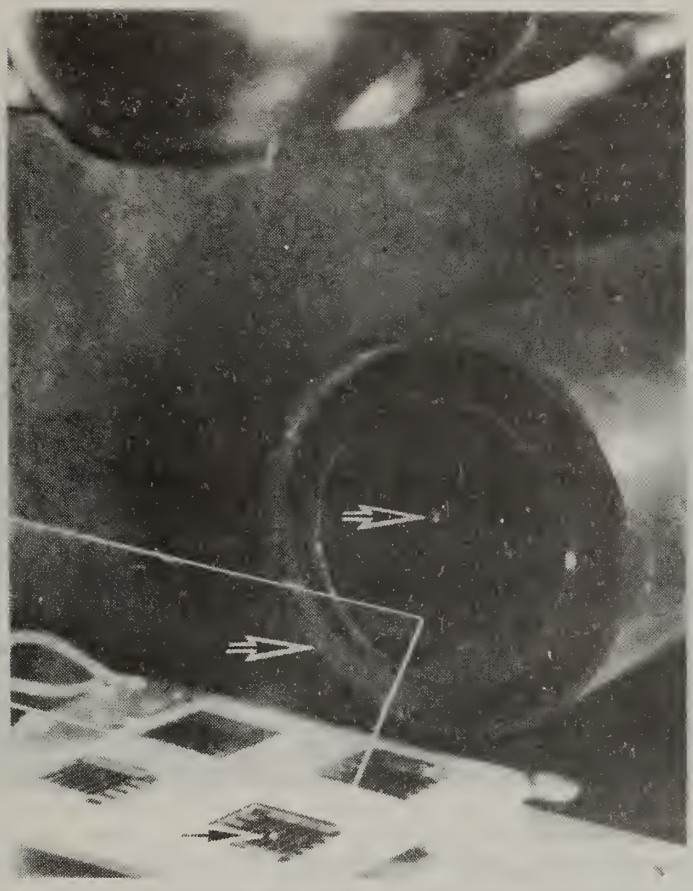

Figure 23. Reflected light configuration with a photomultiplier detector. The laser spot can be seen on the solar cell, the microscope slide reflector, and the filter in front of the detector. The location of the spots are indicated with arrows.

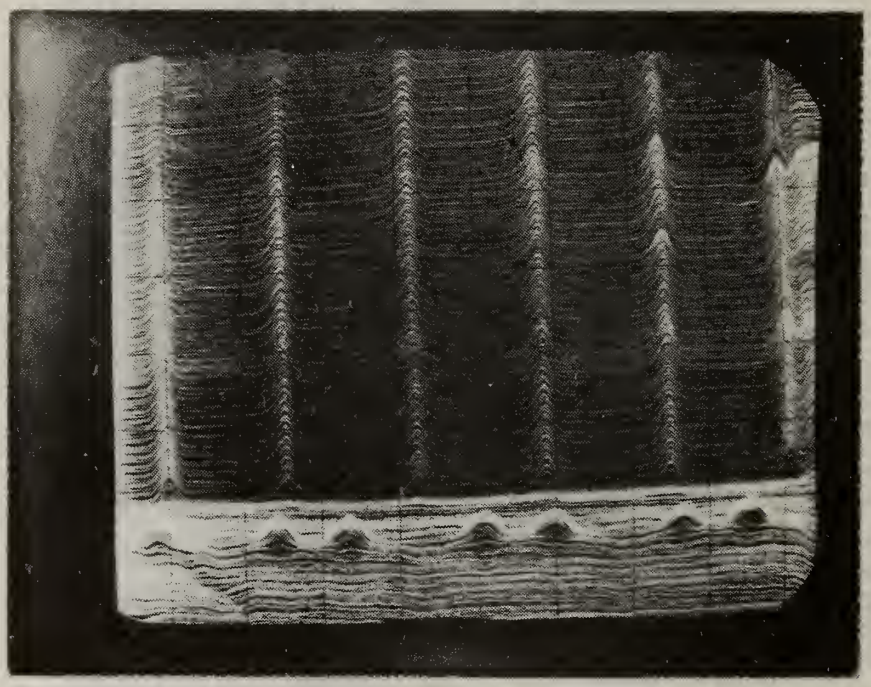

Figure 24. Raster scan of most of an NBS-22 solar cell using the configuration of figure 23 in the large area scan mode of figures 25 and 26. The metallization bus bar is above the area scanned. The lower portion of the scan includes about three and a half arrays of microelectronic test structures. The seven peaks in this portion are due to the pairs of MOS capacitors in each array.

light may also be reflected from the semiconductor surface itself, or from surface laminates, due to optical mismatches. Thus, the reflected-light display signal is a composite of these several images.

Birefringence can be used to detect crystal strain [22] which may be present near regions of material mismatch, e.g., near twin boundaries and near grain boundaries. Strain may cause bandgap dilation or narrowing, and this in turn can influence the minority carrier recombination properties at the interface. Comparison of cell photoresponse scanning measurements with birefringence measurements on a spatial point-by-point basis may help elucidate the interface processes acting to reduce cell conversion efficiencies. This expectation was the motivation for adding the birefringence capability for 1.15-μm scanning.

The light emitted by the 1.15-μm scanning laser is plane-polarized. Detection of bulk birefringence is performed by first extinguishing, through the use of a 1.15-μm analyzer, the light reflected to the photodetector from a scanned flat metal mirror target. This places the axis of the analyzer perpendicular to the plane of polarization of the laser light. The target is then replaced by the cell to be investigated. The cell is (in principle) rotated in the scanning plane, and any resultant intensity variations in the display screen indicate the location of strain-induced birefringence in the cell. It is impractical to rotate solar cell specimens as they are connected for photoresponse measurements made in conjunction with birefringence ones, and so the plane of polarization of the 1.15-μm light is rotated instead. This is accomplished by rotating a half-wave plate in the laser beam; the well-known result of rotating a half-wave plate through an angle of θ in one direction is to cause the plane of polarization of the emerging light to rotate an angle 2θ in the opposite direction.

The scanner microscope has an opening for inserting filters, polarizers, etc. in its body between the ocular and specimen (objective) lenses. A two-aperture, two-position holder was made to slide within this opening. In one position, the optical path is unobstructed. The other position contains a 1.15-μm half-wave plate which can be rotated 360 deg by an external control to rotate the plane of polarization of 1.15-μm scanning light passing through the microscope and incident on the specimen. The analyzer for the reflected light path is in the form of a circular disk fitted with a lever finger, and this fits into a filter-holder slot in the illumination port between the microscope body and the reflected light assembly (see sec. 5.1).

The birefringence apparatus was completed, and a preliminary test was performed during this reporting period. The scanned target was a mirror partially covered with a thin, transparent, plastic sheet. By rotating the half-wave plate in its holder and finding a corresponding orientation of the reflected-light analyzer, it was possible to extinguish the signal from the mirror-only portion while retaining that from the plastic-covered portion, and *vice versa*. Intermediate rotation angles permitted hybrid combinations of the extinguishing-enhancing behavior to be seen, confirming that the apparatus was working as designed.

5.3 A Light Source for Biasing Large-Diameter Cells

A new optical system was developed to replace the fiber optic system when light-biasing large-diameter cells during laser scanning. The fiber optic system uses four fiber-optic bundles to transmit the light from a single quartz-halogen lamp to specimens having dimensions of 2 cm by 2 cm or less. This system is convenient when high power, short working distance lenses are used. This is because the fiber optic ends can be inserted within the limited space between the edge of the objective lens and its scanned specimen, thus placing the light source close to the scanned cell. With cells having diameters larger than about 2 cm, it is not possible to illuminate the cell uniformly using this system. For these larger cells, the entire microscope optics with the exception of the eyepiece, is replaced by a 55-mm focal length single-lens reflex-camera lens (cf sec. 5.4) which yields a 200-mm lens-to-specimen working distance. With the larger working distance, shadowing of the bias light by the scanner optics is not a problem, and the fiber optic light-biasing arrangement can be replaced by a simpler one which illuminates the cell from a longer distance.

A satisfactory illumination system was developed using a pair of 12-V oblong-shaped quartz lamps. These are sold as automobile "passing lights" and are available from most automobile supply houses. Several minor modifications were made to make them suitable for their new service. For their intended application, the lamps are designed to produce parallel light. To achieve this objective, they are assembled with the quartz-halogen bulb in front of, and at the focal point of, a curved metal reflector. A metal shield is clipped to the front of the bulb to ensure that all the light emerging from the lamp is first incident on the reflector. The scanning of large-diameter cells calls for a different configuration. The beam of light from a lamp needs to be about 50 mm in diameter when the lamp is about 300 mm from the scanned cell. This requirement was satisfied by increasing the distance between the bulb and the reflector. This was done by removing the lamp sockets which previously protruded behind the reflector and remounting them so that they also served as spacers between the bulbs and the reflectors. When operated at their new focal length, it was observed that the bulb shields were no longer needed. In fact, their presence caused a decrease in light intensity at the center of the light spot on the specimen. The shields were removed to enhance light uniformity. Additional uniformity of the light with the 50-mm diameter spot was achieved by rotating the bulb sockets 90 deg to place the axis of the bulb filaments parallel to the minor axes of the reflectors.

In addition, the lamps were clamped to the scanner frame to eliminate motion of the lamp relative to the cell specimen due to, e.g., building vibrations which can cause undesired modulation of the bias light. This in turn can mask the response display of the specimen to the (weaker) laser scanning light. By fastening the lamps to the scanner frame, the lamps and specimen tend to move in unison minimizing the undesired light-bias modulation.

Measurements made using a pair of lamps converted in the manner described yielded short-circuit currents in 5-cm diameter single-crystal silicon cells equivalent to about 3 suns insolation.

5.4 Optical Parameters of Various Lens Combinations

Two sets of optical specifications for the NBS laser scanner using different lens combinations are given in tables 3 and 4. The parameters of interest shown in table 3 indicate distances between the objective lens of the system and the sample, and the corresponding total scan excursions possible at this distance. The Zeiss standard research microscope is used with an intermediate body attachment installed between the top of the microscope limb and the body tube holding the eyepiece, which would normally be attached to the top of the limb. The intermediate body holds the polarized light analyzer used in the reflected light mode. The extra distance introduced requires corrector lenses in both the top and bottom of the attachment to maintain the same optics as with the body tube alone. However, if the bottom lens is removed, the spatial resolution of the system is increased, although at the expense of greater working distance. This effect is shown in table 4 for the normal configuration (both lenses in place), and for the modified configuration (bottom lens removed). In all cases, the eyepiece is a 10X ocular lens.

For the movie projector zoom lenses, values are given for the two extremes of the adjustable focal lengths. In the last case listed, the microscope body is omitted, and the 35-mm single-lens reflex camera lens is installed to provide a wider area of scan. More detailed illustrations of this system are given in figures 25 and 26.

Table 4 extends the optical data for some of the combinations of table 3 and adds five others. The first four columns give the scanner resolution measured with a standard calibrated grid. The resolution, a measure of effective laser spot size, is obtained from the relative intensity of transmitted light through the mask between opaque grid lines for various grid spacings. The resolution stated in micrometers is the width of the openings between grid lines of the calibrated grid which provides a value of the modulation percentage which falls within the range of about 20 to 40 percent. The modulation percentage is defined as 100 times the ratio x/y where x is the peak-to-peak variation in the transmitted light intensity as the laser spot is scanned across the grid, and y is the unobstructed intensity of the laser spot. At an extreme, 100-percent modulation corresponds to all the laser spot being transmitted between the opaque grid lines. A more detailed description of the measurement is given in elsewhere [23].

Columns 5 and 6 of table 4 give, in arbitrary units, the relative amount of light reflected from the objective lenses themselves. The measurements were made with a black piece of paper at the sample position and the reflected light recorded by the system shown in figure 25. This illustrates an important consideration: in the reflected-light mode, light reflected from the surfaces of the optical elements themselves introduces an interference into the solar cell scanning measurements. A value of 50 or less in this table gives satisfactory performance; however, this generic problem suggests that mirrors may be preferred as optical elements wherever possible. It is seen that the problem is worse for the infrared light than for the visible beam.

Table 3. NBS Laser Scanner Specimen to Objective-Lens Working Distance and Scan Excursion for the 0.633-μm Laser Wavelength Tabulated Using a 10X Ocular Lens, a Total Optical Scanning Angle of 20 Deg at the Ocular Lens, and with Various Objective Lenses.

Objective Lens	Microscope in Normal Service (1) Working Distance (mm)	Scan Excursion (2) (mm)	Microscope Modified (3) Working Distance (mm)	Scan Excursion (2) (mm)	Remarks
Zeiss Epiplan 4/.1	10	2.2	0	3.5	
Zeiss Epiplan 2.5/.1	6	3.3	-	-	
Rolyn Rau 2.5/.1	77	6.0	47	5.0	
Rolyn Rau 1/.06	75	4.5	47	6.0	
"Super 8" Movie Proj.	16	2.2	11	3.0	20 mm F.L.
Lens, F/1.4, 20-32 mm F.L.	21	3.3	13	4.8	32 mm F.L.
"Standard 8" Movie Proj.	12	2.1	10	3.0	20 mm F.L.
Lens, F/1.4, 20-32 mm F.L.	17	3.2	12	4.8	32 mm F.L.
Projector Lens F/2.8, 75 mm F.L.	200 (4)	11.0	77	11.5	
Fujion 35 mm SLR Lens, F/2.2, 55 mm F.L.	-	-	280	50	(5)

Notes: (1) Both lenses in microscope body retained.
(2) May be necessary to remove reflected-light beam splitter to prevent scan cropping.
(3) Bottom lens in microscope body removed.
(4) Exceeds objective-lens-to-specimen-stage maximum working distance.
(5) Microscope not used. Optical configuration shown in figures 25 and 26.

Table 4. NBS Laser Scanner Scanning Resolution and Reflected-Light Bias, for 0.633- and 1.15-μm Laser Wavelengths Tabulated Using a 10X Ocular Lens and with Various Objective Lenses.

Objective Lens	Resolution (4) for Stated Modulation Percentage				Relative Reflected-Light (5)		Remarks
	Normal (2)		Modified (3)				
	0.633 μm (μm)	1.15 μm (μm)	0.633 μm (μm)	1.15 μm (μm)	0.633 μm (arbitrary units)	1.15 μm	
Zeiss Epiplan 40/.60	1.0 at 30%	2.0 at 45%	1.0 at 36%	1.58 at 30%	-	40	
Zeiss Epiplan 16/.35	1.6 at 30%	2.0 at 35%	1.6 at 35%	2.0 at 30%	20	40	
Zeiss Epiplan 8/.2	2.5 at 45%	4.0 at 25%	2.5 at 25%	4.0 at 20%	30	170	
Zeiss Epiplan 4/.1	5.0 at 40%	6.3 at 25%			70	2,300	
Rolyn Rau 2.5/.1 (6)	10.0 at 40%	12.5 at 35%	10.0 at 35%	10.0 at 21%	40	40	
Rolyn Rau 1/.06	12.5 at 32%	20.0 at 30%	5.0 at 20%	10.0 at 27%	90	69	
"Super 8" Movie Proj.	2.5 at 25%	-	2.5 at 20%	4.0 at 20%	100	170	20 mm F.L.
Lens, F/1.4, 20-32 mm F.L.	3.16 at 20%	-	4 at 26%	5.0 at 14%	60	80	32 mm F.L.
"Super 8" Movie Proj.	2.5 at 25%	-	2.5 at 22%	4.0 at 22%	100	120	20 mm F.L.
Lens, F/1.5, 20-32 mm F.L.	4.0 at 28%	-	3.2 at 30%	5.0 at 18%	65	60	32 mm F.L.
"Standard 8" Movie Proj.	4.0 at 24%	-	2.5 at 23%	4.0 at 21%	125	240	20 mm F.L.
Lens, F/1.4, 20-32 mm F.L.	5.0 at 30%	-	4.0 at 22%	5.0 at 15%	70	130	32 mm F.L.
"Computer" Vidicon Lens, F/2.8, 25 mm F.L.	4.0 at 30%	5.0 at 20%	3.2 at 30%	5.0 at 25%	50	70	
Projector Lens, F/2.8, 75 mm F.L.	NA	NA	10.0 at 19%	NA	80	260	

NOTES: (1) 0.633-μm value, slightly greater for 1.15 μm.
(2) Both lenses in microscope body retained.
(3) Bottom lens in microscope body removed.
(4) Resolution = linewidth of calibrated grid, for which the modulation percentage falls within the range of about 20 to 40%.

$$\text{Modulation Percentage} = 100\,\frac{y_{\%}}{x}$$

where: x = peak-to-peak variation in transmitted light intensity across the calibrated grid and
y = total intensity of laser spot.

(5) Due to reflections from objective lens surfaces.
(6) Long objective.

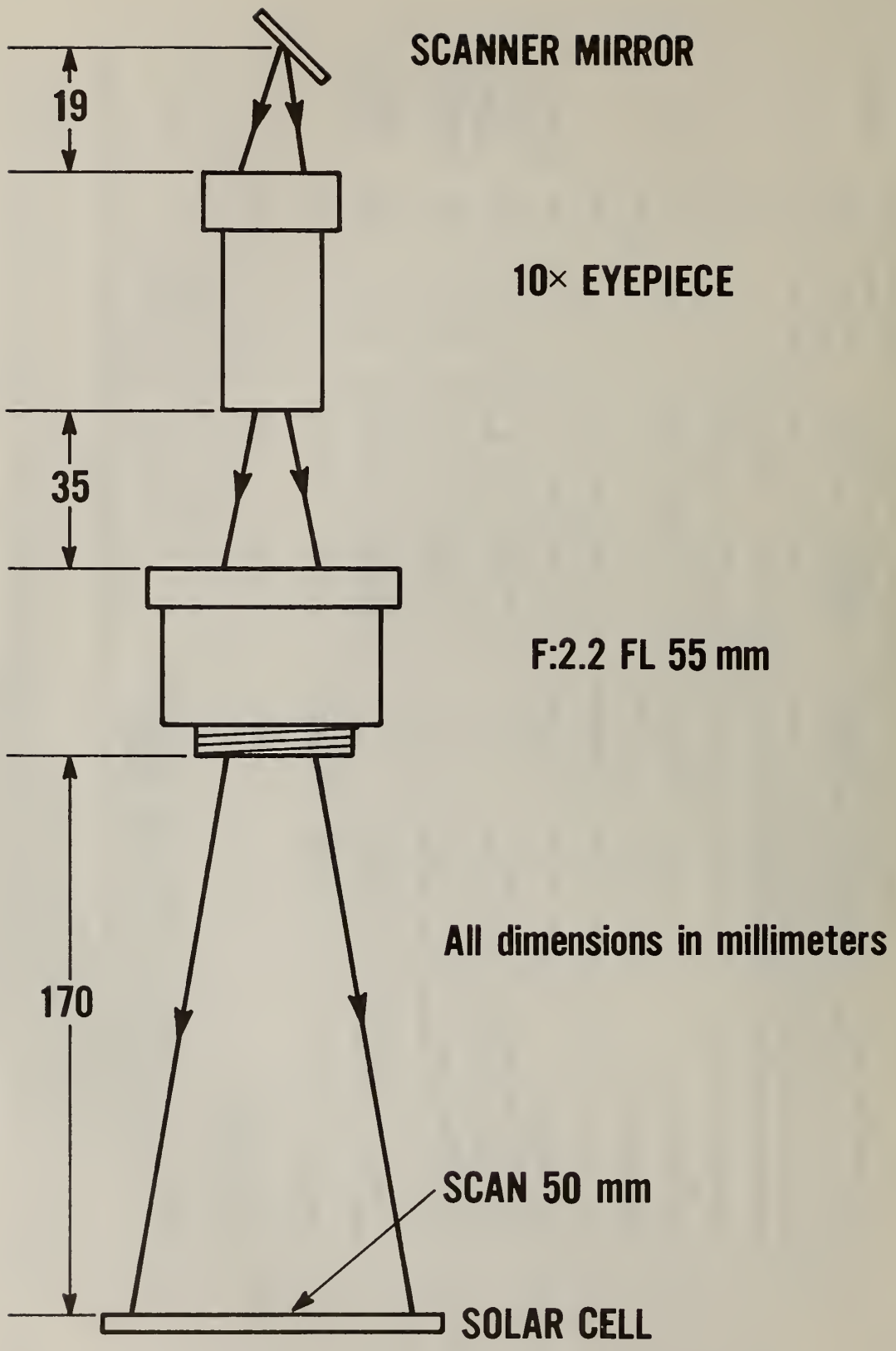

Figure 25. Optical diagram for the large area scan configuration.

Figure 26. Photograph of the large area scan configuration.

5.5 Variable Specimen Temperature

One of the project objectives is to develop techniques which, when used in conjunction with the laser scanner and other measurement methods, can be used to separate the several phenomena which may be operating in concert at grain boundaries to reduce the conversion efficiency of polycrystalline silicon solar cells. A classic method for analyzing the physical behavior of experimental specimens is to perform appropriate measurements as a function of specimen temperature. Toward this objective, solar cell heating and cooling stages were constructed to fit between the scanned specimen and the specimen translation stage of the microscope.

5.5.1 Heating Stage

The heater stage has a temperature range from room temperature to about 160°C, that is, to slightly below the eutectic temperature (183°C) of the lead-tin solder commonly used for cell contacts. The stage was built around a commercially available heater element sold as a substrate heater for a thermocompression bonder, which is designed to be energized from a dc source and maintained at the desired temperature by an on-off controller. The heater element is rectangular and measures 3.75 cm by 6.25 cm and 2.5 cm thick. To fit it for scanner service, it was only necessary to thermally insulate the heater from the specimen translation stage. This was done by bonding, with silicone rubber, a 2.5-cm thick block of plastic foam to the base of the heater. Temperatures are readily set and maintained to $\pm$0.5°C over the desired range. No problems were encountered using the 0.633-μm source. Some controller noise, due to on-off heater current transients, was observed on the scanner display screen when the weaker 1.15-μm cell photosignals were displayed. This annoyance may perhaps be eliminated by changing the controller to a zero-crossing type.

5.5.2 Cooling Stage, Thermoelectric Type

A stage for cooling specimens over the range from room temperature to -20°C was constructed using a flat, single-stage themoelectric element having the dimensions 3.75 cm by 3.75 cm and 1 cm thick. The thermoelectric element is energized by an adjustable, low-voltage, direct-current source and cools by pumping heat from the top surface on which the specimen is mounted to the bottom surface. The specifications for the element place an upper limit on the temperature of the bottom surface. In order to achieve the desired cooling range without exceeding the rated bottom surface temperature, one must place this surface in thermal contact with a heat sink. A water-cooled copper block was constructed to serve this purpose. Adequate thermal contact between the thermoelectric element and the copper block is achieved by lightly coating the lower surface of the element with silicone "heat sink" grease and bolting the two units together. This assembly is set into the cut-out portion of a plastic-foam disk 9.50 cm in diameter and 3.1 cm thick. The disk and a specimen cover prevent moisture in the room air from condensing on the scanned specimen; the small-scale effect of condensation (which occurs at temperatures at and below the dew point) is to coat the specimen with a multitude of tiny water "lenses" which degrades the optical scanning resolution. The specimen cover is a clear plastic dish through which dry nitrogen is flowed to eliminate this problem.

The cooling stage worked satisfactorily and was used to cool specimens between room temperature and about -2°C without dry nitrogen flow while they were laser scanned using both 0.633- and 1.15-μm wavelengths.

5.5.3 Cooling Stage, Compressor Type

At the suggestion of Dr. R. A. Forman of the Electron Devices Division, a means for cooling specimens over the range of from room temperature to about -60°C was constructed using a commercially available refrigerator compressor. The compressor is hermetically sealed to a stainless steel flexible tube with an outer diameter (OD) of about 1.0 cm. This tube is coaxial to allow the liquid refrigerant to be pumped through the center capillary to the tip of the tube where its refrigerant expands to a gas. The expanding gas absorbs best from the tube, cooling it, as the gas returns to the compressor through the outer portion of the coaxial line. The flexible tube is coiled into a 3.7-cm deep circular channel cut into the bottom of a solid cylindrical aluminum block which is 4.7 cm high and 10.2 cm in diameter. The OD of the channel is 8.8 cm and the width of the channel is just large enough to accommodate the flexible tube. A groove, cut into the bottom edge of the wall formed by the channel, allows the extension of the flexible tube to exit from the aluminum block. A circular aluminum plate, 0.35 cm thick, is screwed to the bottom of the block to contain the coiled tube. The volume remaining in the channel that is not occupied by the tube is filled with silicone mixed with copper powder to enhance the thermal conductance between the tube and the block.

The top of the block is provided with screw holes for use in bolting a specimen holder to the block. Also on the top of the block is a slightly flattened 0.5-cm OD copper tube. This tube is sealed at one end and is bent and fastened in such a way that it circles the area on the block for the specimen holder and has the open end extend out from the side of the block. Distributed on the top of the circular portion of the tube are small diameter holes. The purpose of this tube is to conduct dry nitrogen into the specimen chamber which is formed by placing a plastic cover over the top of the aluminum block. To thermally insulate the chamber, the plastic cover is fitted with plastic foam. The cover contact to the block is by way of the plastic foam which is such that it allows the nitrogen introduced into the chamber to escape. The cover is also fitted with a clear plastic window which is situated centrally to allow for the entrance of the laser beam from the scanner. The purpose of the dry nitrogen is to prevent frosting inside the specimen chamber. A similar approach is used to prevent frosting on the top side of the window. A thin-walled tube, 0.3 cm OD, was bent and fastened so that it circles the top side of the specimen window. Holes in the tube, 0.15 cm in diameter, face to the center so as to direct the dry nitrogen over the face of the window. The tube is, in turn, covered by an inverted plastic cup 0.7 cm high and 6.6 cm in diameter which has a circular hole cut to allow for the escape of the nitrogen. The hole is of such a size that its diameter is somewhat larger than the window but smaller than the diameter of the circle that the tube forms. This is to help guide the dry nitrogen over the window.

With the aluminum block encased in plastic foam material and with a low-pressure dry nitrogen source for each of the above described tubes, the

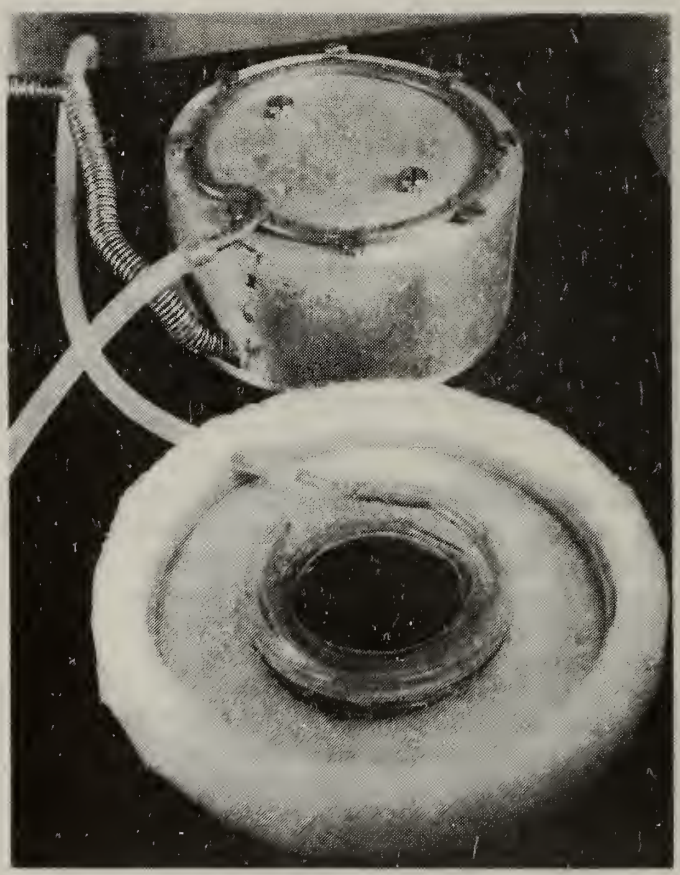

Figure 27. Photograph of the compressor type cooling stage (top) and cover (bottom).

cooling stage was able to cool specimens to as low as -60°C with no frosting or condensation on the optical parts or the specimen. A photograph of the cooling stage without the insulation around the aluminum block is shown in the upper part of figure 27 and the top cover is shown in the lower part.

6. WORKSHOPS

6.1 Stability of (Thin Film) Solar Cells and Materials

The proceedings of the Workshop on Stability of (Thin Film) Solar Cells and Materials, held May 1-3 1978 at NBS, were published [1], as was a companion document which summarized the conclusions of this workshop and their implications [2]. The orientation of the workshop and the topics addressed were discussed in the previous annual report [24].

6.2 Photovoltaic Material and Device Measurements

The Photovoltaic Material and Device Measurements Workshop (with focus on polycrystalline thin film cells) was held June 11-13, 1979 in Arlington, Virginia with 210 registrants. The workshop was conducted for the Department of Energy by the Photovoltaics Program Office of SERI in association with the Electron Devices Division of NBS. The general purpose of the workshop was to accelerate the development of thin film cells by improving the versatility and reliability of material and device measurement techniques. No workshop proceedings were issued as such, but contributions from presenters at the workshop have been the subject of two special issues of the journal, *Solar Cells* [25]. The preface to these issues, by D. E. Sawyer as Guest Editor, and their tables of contents, are provided in Appendix B.

7. CONSULTATION AND LIAISON ACTIVITIES

7.1 Consultations to SERI

At the suggestion of the SERI PVPO, D. E. Sawyer attended the December 18, 1978 Photovoltaics Session of the Workshop on Reliability of Materials for Solar Energy at Denver, Colorado and participated in the session discussions. The workshop was organized by the Materials Branch of SERI's Research Division.

D. E. Sawyer evaluated for the PVPO four measurements-related proposals which they received under their Innovative Concepts Solicitation, and one unsolicited proposal.

A number of activities were engaged in by D. E. Sawyer and H. K. Kessler to aid the PVPO in duplicating the NBS laser scanner for routine evaluation of cell specimens provided the PVPO by PVPO contractors. These activities include sending the PVPO detailed information on the NBS scanner parts and appropriate NBS publications and copies of the scanning resolution tables (table 4 and 5). Reviews and discussions of the theory, construction, and use of the scanner were held during visits of D. E. Sawyer to the PVPO and during visits of SERI PVPO personnel to NBS. The latter visits are listed below:

April 1979 – Mr. Richard Matson of the Solar Energy Research Institute (SERI) (Golden, CO) visited D. E. Sawyer and H. K. Kessler to discuss the Photovoltaic Program Offices (PVPO) project to set up a laser scanner at SERI similar to the one at NBS.

May 1979 – Mr. Phil Pierce of SERI (Golden, CO) visited D. E. Sawyer to discuss the photovoltaic program conducted at NBS for SERI.

June 1979 – Dr. Robert Lewis of PVPO, SERI (Golden CO) visited D. E. Sawyer to discuss applications of laser scanner to SERI's needs.

June 1979 – Mr. Alan Postlethwaite, program manager in the DOE Photovoltaic Office (Washington, DC), visited D. E. Sawyer and H. K. Kessler to see the laser scanner and discuss its use in photovoltaic work.

July 1979 – Mr. Ted Cannon and Mr. Clyde Carter of SERI (Golden, CO) visited D. E. Sawyer, H. K. Kessler, and H. A. Schafft to see the laser scanner in operation and to familiarize themselves with the apparatus.

7.2 Visits from Industry and Universities to the National Bureau of Standards

The following visits and consultations were conducted with the authors:

Dec. 1978 – Drs. George Storti and John Wohlgemuth of Solarex (Rockville, Maryland) visited D. E. Sawyer and H. K. Kessler to conduct laser scanning on experimental polycrystalline and vertical junction solar cells being developed under DoE sponsorship.

Jan. 1979 – Professor Wayne Anderson, SUNY (Buffalo, New York), and Alan E. Delahoy, a graduate student at Rutgers University (New Brunswick, New Jersey), visited to scan experimental solar cells.

Jan. 1979 – Walter Manson of Texas Instruments (Dallas, Texas) visited D. E. Sawyer and H. K. Kessler and performed measurements on experimental tandem junction solar cells.

Feb. 1979 – George Storti and Scott Johnson of Solarex visited for further discussions on laser scanning of solar cells being developed under DoE/SERI sponsorship.

Feb. 1979 – Brian Plunkett and Patrick Lasswell of the Institute for Energy Conversion, University of Delaware (Wilmington, Delaware), worked with Sawyer and Kessler on techniques for laser scanning exploratory CdS/Cu_2S and Cd(Zn)S/Cu_2S solar cells being developed under SERI sponsorship.

Feb. 1979 – Masashi Nagasi, VLSI Technology Research Association Cooperative Labs, visited to discuss the laser scanner.

Mar. 1979 – Brian Plunkett and Patrick Lasswell, Institute for Energy Conversion, visited NBS to study equipment and techniques for laser scanning exploratory CdS/Cu_2S and Zn_3P_2 solar cells and test specimens being developed under SERI sponsorship.

Mar. 1979 – Mr. William Morris, staff engineer at the Electronics Laboratory, General Electric Co. (Syracuse, New York), visited D. E. Sawyer, D. W. Berning, and H. K. Kessler. He is compiling a failure-analysis handbook for the Rome Air Development Command, New York and expressed considerable interest in the scanning techniques developed for this application and also for device design for determining processing-related defects.

Apr. 1979 – Dr. Douglas Yates of Mobil Tyco Solar Energy Corporation (Waltham, Massachusetts) visited NBS to make laser scanner measurements on EFG samples.

Apr. 1979 – David Lischnow of Bell Laboratories (Allentown, Pennsylvania) visited D. W. Berning. Mr. Berning assisted Mr. Lischnow in finding inverted regions in transistors they had made by using the laser scanner.

June 1979 – Dr. Gary Turner of ARCO-Solar (Chatsworth, California) visited Dr. Sawyer to study the laser scanner prior to constructing his own and to exchange cell measurement techniques.

Aug. and Nov. 1979 – Dr. Douglas Yates of Mobil Tyco made two additional visits to conduct further laser scanner studies on silicon EFG solar cells manufactured by his company.

REFERENCES

1. Sawyer, D. E., and Schafft, H. A., Eds., *Semiconductor Measurement Technology:* NBS/DOE Workshop, Stability of (Thin Film) Solar Cells and Materials, NBS Spec. Publ. 400-58 (August 1979).

2. Schafft, H. A., and Sawyer, D. E., A Perspective of a Workshop on Stability of (Thin Film) Solar Cells and Materials, NBSIR 79-1778 (July 1979).

3. Convers Wyeth, N., and Catalano, A., Spectral Response Measurements of Minority-Carrier Diffusion Length in Zn_3P_2, *J. Appl. Phys.* 50, 1403-1407 (1979).

4. Catalano, A., private communication.

5. Carbajal, B. G., High Efficiency Cell Development, DOE/JPL/954881-5, Final Technical Progress Report (1978).

6. Lehovec, K., and Fedotowsky, A., Scanning Light Spot Analysis of Faulty Solar Cells, *Solid-State Electronics* 23, 565-576 (June 1980).

7. Sawyer, D. E., Kessler, H., and Schafft, H. A., Measurement Techniques for Solar Cells, Quarterly Report: April 1 to June 30, 1978, NBSIR 79-1909 (November 1979), pp. 12-18.

8. Yates, D. A., private communication.

9. Lanyon, H. P. D., Bandgap Narrowing in Moderately to Heavily Doped Silicon, *IEEE Trans. Electron Devices* ED-26, 1014-1018 (1979).

10. Mahan, G. D., Energy Gap in Si and Ge: Impurity Dependence, *J. Appl. Phys.* 51, 2634-2646 (1980).

11. Lowney, J. R., Kahn, A. H., Blue, J. L., and Wilson, C. L., Disappearance of Impurity Levels in Si and Ge Due to Screening, to be published in *J. Appl. Phys.*

12. Turner, G. W., Fan, J. C. C., and Salerno, J. P., Infrared Electroluminescence as a Diagnostic Tool for Polycrystalline GaAs Solar Cells, *Solar Cells* 1 (3), 261-262 (May 1980)

13. Lehovec, K., and Fedotowsky, A., Solar Cell Mathematical Analysis and Computer Simulation, NBS-GCR-285 (February 1981).

14. Buehler, M. G., Grant, S. D., and Thurber, W. R., Bridge and van der Pauw Sheet Resistors for Characterizing the Line Width of Conducting Layers, *J. Electrochem. Soc.* 125, 650-654 (1978).

15. Buehler, M. G., *Semiconductor Measurement Technology:* Microelectronic Test Pattern NBS-3 for Evaluating the Resistivity-Dopant Density Relationship of Silicon, NBS Spec. Publ. 400-22 (May 1976), p. 13.

16. Buehler, M. G., and Thurber, W. R., A Planar Four-Probe Test Structure for Measuring Bulk Resistivity, *IEEE Trans. Electron Devices* ED-23, 968-974 (1976).

17. Sze, S. M., *Physics of Semiconductor Devices*, pp. 444-467 (John Wiley & Sons, New York, 1969).

18. Buehler, M. G., The D-C MOSFET Dopant Profile Method, *J. Electrochem. Soc.* 127, 701-704 (1980).

19. Sah, C. T., Detection of Recombination Centers in Solar Cells from Junction Capacitance Transients, *IEEE Trans. Electron Devices* ED-24, 410-419 (1977).

20. Russell, T. J., Maxwell, D. B., Reimann, C. T., and Buehler, M. G., A Microelectronic Test Pattern for Measuring Uniformity of an Integrated Circuit Fabrication Technology, *Solid State Technology* 22 (2), 71-74 (1979).

21. Buehler, M. G., Comprehensive Test Patterns with Modular Test Structures: The 2 by N Probe-Pad Array Approach, *Solid State Technology* 22 (10), 89 (1979).

22. Jessop, H. T., and Harris, F. C., *Photoelasticity, Principles and Methods* (Dover Publications, New York, 1950).

23. Sawyer, D. E., and Berning, D. W., *Semiconductor Measurement Technology:* A Laser Scanner for Semiconductor Devices, NBS Spec. Publ. 400-24 (February 1977).

24. Sawyer, D. E., Kessler, H. K., and Schafft, H. A., Measurement Techniques for Solar Cells: Annual Report for the Period September 15, 1977 to December 14, 1978, NBSIR 80-2027 (July 1980).

25. *Solar Cells* 1 (2) (February 1980) and 2 (3) (May 1980).

APPENDIX A

Associated Publications

A.1 Publications

Schafft, H. A., and Sawyer, D. E., A Perspective of a Workshop on Stability of (Thin Film) Solar Cells and Materials, NBSIR 79-1778 (July 1979).

Sawyer, D. E., and Schafft, H. A., Eds., *Semiconductor Measurement Technology:* NBS/DoE Workshop, Stability of (Thin Film) Solar Cells and Materials, NBS Spec. Publ. 400-58 (August 1979).

Sawyer, D. E., Kessler, H. K., and Schafft, H. A., Measurement Techniques for Solar Cells, Quarterly Report, April 1 to June 30, 1978, NBSIR 79-1909 (October 1979).

Sawyer, D. E., Kessler, H. K., and Schafft, H. A., Measurement Technologies for Solar Cells, Annual Report, September 15, 1977 to December 14, 1978, NBSIR 80-2027 (July 1980).

Lehovec, K., and Fedotowsky, A., Scanning Light Spot Analysis of Faulty Solar Cells, *Solid-State Electronics* 23, 565-576 (June 1980).

A.2 Patent Applications

Sawyer, D. E., Nondamaging Technique for Locating Semiconductor Device Defects and Measuring Device Resistances, United States Patent and Trademark Office (filed May 25, 1979).

APPENDIX B

Preface to
Solar Cells
Volume 1, February 1980

The papers in this special issue were selected by peer review from those submitted following their presentation at the first meeting of the Photovoltaic Material and Device Measurements Workshop held in Arlington, Virginia, U.S.A., June 11-13, 1979. The general purpose of these workshops, conducted for the U.S. Department of Energy by the Photovoltaics Program Office of the Solar Energy Research Institute, Golden, Colorado, is to accelerate the development of thin film solar cells by improving the versatility and reliability of terrestrial solar cell material and device measurement techniques. This first workshop, conducted in association with the U.S. National Bureau of Standards, Washington, DC, focused on polycrystalline materials and the associated thin film cells. Workshops to examine other photovoltaic materials and/or technologies will be held in the future.

The subjects included in the first "measurements" workshop, and thus the topics treated in this special issue, were selected based on questionnaires distributed at the Department of Energy's Photovoltaic R&D Review Meeting held on October 24-26, 1978, Vail, Colorado. The attendees, who represented the forefront workers in the U.S. thin film photovoltaic community, were asked for their measurement needs and concerns, and the workshop was constructed accordingly. Because of this genesis, photovoltaic researchers throughout the world should find the papers which follow to be timely and of great interest.

David E. Sawyer, Guest Editor
Electron Devices Division
National Bureau of Standards
Washington, DC 20234

SOLAR CELLS, Vol. 1, No. 2 February 1980

CONTENTS

Preface 113

*Perspective on photovoltaic material and device measurements 115
A. Rothwarf (Newark, Del., U.S.A.)

Measuring trace elements in semiconductors: methods and pitfalls . . 117
R. M. Lindstrom (Washington, D.C., U.S.A.)

Electron-beam-induced current characterization of polycrystalline silicon solar cells 123
J. I. Hanoka (Waltham, Mass., U.S.A.)

*Backscattering and transmission electron microscopy studies of layered structures 141
J. W. Mayer (Pasadena, Calif., U.S.A.)

*New techniques for the study and control of grain boundary effects 145
R. F. Wood, R. T. Young, R. D. Westbrook, J. Narayan, W. H. Cristie, and J. W. Cleland (Oak Ridge, Tenn., U.S.A.)

*Grain size and its influence on efficiency in polycrystalline GaAs solar cells 149
A. E. Blakeslee and S. M. Vernon (Yorktown Heights, N.Y., U.S.A.)

*Characterization of EFG silicon ribbons by ion beam techniques . . . 153
M. Hage-Ali, R. Stuck, M. Toulemonde, and P. Siffert (Strasbourg, France)

*Structural and chemical characterization of photovoltaic materials and devices 158
J. D. Meakin (Newark, Del., U.S.A.)

The $Zn_xCd_{1-x}S/Cu_2S$ heterojunction: review and recent measurements 159
L. C. Burton (Blacksburg, Va., U.S.A.)

Scanning light spot analysis of faulty solar cells 175
K. Lehovec and A. Fedotowsky (Los Angeles, Calif., U.S.A)

*Correlation of grain boundary electrical properties with grain boundary impurities in multigrained silicon using surface analytical techniques 178
L. L. Kazmerski and P. J. Ireland (Golden, Colo., U.S.A.)

* Extended abstract.

Etching of CdS films 183
F. A. Shirland (Pittsburgh, Pa., U.S.A.)

Effect of substrate orientation on the properties of the Si/PbS heterojunction 199
H. Elabd, A. J. Steckl, and W. Vidinski (Troy, N.Y., U.S.A.)

*Photoconductivity as a probe of polycrystalline films 209
R. H. Bube (Stanford, Calif., U.S.A.)

*Optical properties of polycrystalline semiconductor films 213
A. H. Clark (Orono, Me., U.S.A.)

*Electronic transport and optical properties of dislocations in deformed compound semiconductors 216
C. Elbaum (Providence, R.I., U.S.A.)

*Electron diffusion lengths in the CdS/Cu_xS cell from spectral response measurements 218
C. Moses (Canton, N.Y., U.S.A.) and D. Wasserman (Ithaca, N.Y., U.S.A.)

*Effective diffusion length in polycrystalline semiconductor thin films 222
T. L. Chu, E. D. Stokes, and S. S. Chu (Dallas, Tex., U.S.A.)

The design and utilization of microprocessor-controlled absolute spectral response system 225
L. M. Kilgren, N. C. Wyeth, and W. E. Devaney (Newark, Del., U.S.A.)

*Electron-beam-induced current and scanning light spot techniques for investigating the response of polycrystalline solar cells 233
N. Inoue, S. M. Goodnick, and C. W. Wilmsen (Fort Collins, Colo., U.S.A.)

SOLAR CELLS, Vol. 1, No. 3 May 1980

CONTENTS

Some investigations on the influence of defects/grain boundaries on photovoltaic mechanisms in polycrystalline silicon films 237
B. L. Sopori and A. Baghdadi (Phoenix, Ariz., U.S.A.)

Scanned laser response studies of metal-insulator-silicon solar cells in polycrystalline Czochralski silicon 251
J. R. Szedon, T. A. Temofonte, and T. W. O'Keeffe (Pittsburgh, Pa., U.S.A.)

*Infrared electroluminescence as a diagnostic tool for polycrystalline GaAs solar cells 261
G. W. Turner, J. C. C. Fan, and J. P. Salerno (Lexington, Mass., U.S.A.)

Study of grain boundaries in GaAs by scanning light microscopy . . . 263
R. M. Fletcher, D. K. Wagner, and J. M. Ballantyne (Ithaca, N.Y., U.S.A.)

*Diffusion length measurements in Cu_2S 271
W. J. Biter and T. W. O'Keeffe (Pittsburgh, Pa., U.S.A.)

*Ellipsometry of thin silicon dioxide films on rough polycrystalline silicon surfaces 272
T. D. Burleigh, S. Wagner, and T. F. Ciszek (Golden, Colo., U.S.A.)

*Evaluation of silicon-on-ceramic using light-beam-induced currents 273
J. D. Zook (Bloomington, Minn., U.S.A.)

Experimental determination of the photon economy in polycrystalline thin film photovoltaic materials and devices 275
J. A. Bragagnolo and E. A. Fagen (Newark, Del., U.S.A.)

Grain boundary defects in thin semicrystalline material 285
Z. C. Putney and W. F. Regnault (Gaithersburg, Md., U.S.A.)

*Barrier heights and passivation of grain boundaries in polycrystalline silicon 293
C. H. Seager and D. S. Ginley (Albuquerque, N.M., U.S.A.)

*Electrical transport properties in inhomogeneous media 297
R. Landauer (Yorktown Heights, N.Y., U.S.A.)

*Grain boundary resistance measurements in polycrystalline GaAs . . . 298
M. J. Cohen, J. S. Harris, Jr., and J. R. Waldrop (Thousand Oaks Calif., U.S.A.)

* Extended abstract.

*Physical models for recombination currents in polycrystalline silicon p-n junction solar cells 302
J. G. Fossum, A. Neugroschel, F. A. Lindholm, and J. A. Mazer Gainesville, Fla., U.S.A.)

*Effect of interface recombination at p-n junction perimeters on photoluminescence and current 304
C. H. Henry (Murray Hill, N.J., U.S.A.)

Grain boundary effects and conduction mechanism studies in chromium metal-insulator-silicon solar cells on polycrystalline silicon . . . 305
W. A. Anderson, K. Rajkanan (Buffalo, N.Y., U.S.A.), A. E. Delahoy, and S. L. Hyland (Piscataway, N.J., U.S.A.)

*Study of spatial inhomogeneities in photosensitive materials using direct current and microwave techniques 311
P. Herczfeld, L. Hanlon, and J. Wargin (Philadelphia, Pa., U.S.A.)

Noise spectral density as a device reliability estimator 315
J. DuBow and C. Osterwald (Fort Collins, Colo., U.S.A.)

*Capacitance as a tool for investigating thin film CdS/Cud$_2$S heterojunctions 321
W. J. Manthey and N. C. Wyeth (Newark, Del., U.S.A.)

*Measurement of the resistivity of thin CdS films on brass substrates 323
S. Hogan, S. Wagner (Golden, Colo., U.S.A.), and F. Barnes (Boulder, Colo., U.S.A.)

Measurement techniques in thin film polycrystalline materials and devices (solar cells) 327
H. K. Charles, Jr., R. J. King, and A. P. Ariotedjo (McLean, Va., U.S.A.)

NBS-114A (REV. 2-8C)

U.S. DEPT. OF COMM. BIBLIOGRAPHIC DATA SHEET (See instructions)	1. PUBLICATION OR REPORT NO. NBSIR 80-2181	2. Performing Organ. Report No.	3. Publication Date January 1981

4. TITLE AND SUBTITLE

Measurement Techniques for Solar Cells, Annual Report
December 15, 1978 to December 14, 1979

5. AUTHOR(S)

D. E. Sawyer, H. K. Kessler, T. J. Russell, W. F. Lankford, and H. A. Schafft

6. PERFORMING ORGANIZATION (If joint or other than NBS, see instructions)

NATIONAL BUREAU OF STANDARDS
DEPARTMENT OF COMMERCE
WASHINGTON, D.C. 20234

7. Contract/Grant No.

Task Order AO54SE

8. Type of Report & Period Covered

Final, Dec. 15, 1978 to Dec. 14, 1979

9. SPONSORING ORGANIZATION NAME AND COMPLETE ADDRESS (Street, City, State, ZIP)

Solar Energy Research Institute
1617 Cole Boulevard
Golden, CO 80401

10. SUPPLEMENTARY NOTES

[ ] Document describes a computer program; SF-185, FIPS Software Summary, is attached.

11. ABSTRACT (A 200-word or less factual summary of most significant information. If document includes a significant bibliography or literature survey, mention it here)

The NBS-developed laser scanner was used to examine a variety of devices: Cu_2S/CdS cells, silicon tandem junction cells, Zn_3P_2 Schottky diode specimens, and edge-fed growth polycrystalline silicon cells. The results show that it is possible to detect cell design- and processing-induced losses in conversion efficiency, areas of missing antireflection coating, lack of ohmic contact of the metallization to the cell, breaks in cell metallization fingers, fine cracks, scratches, and silicon carbide inclusions. Observation of photoresponse caused by point shunts in the junction and cell cracks is consistent with modeling work. A solar cell test pattern is described and the results of cell sheet resistance measurements are discussed. The test pattern includes four solar cells (three with intentional defects). It also includes microelectronic test structures to determine certain material and design characteristics of these cells. The test pattern serves as a vehicle for linking theoretical and experimental results and placing the scanner technique on a firm theoretical base. Modifications to the laser scanner system are described including an improved reflected-light detection system, a birefringence capability, temperature-controlled stages for heating (to 160°C) and cooling (to -60°), and a new light source for biasing large-diameter cells. Support to the Photovoltaic Program Office of the Solar Energy Research Institute through the conduct of workshops, consultations, and liaison activities is described.

12. KEY WORDS (Six to twelve entries; alphabetical order; capitalize only proper names; and separate key words by semicolons)

Defect identification; laser scanner; measurement techniques; photovoltaics; solar cells; test pattern.

13. AVAILABILITY

[X] Unlimited

[ ] For Official Distribution. Do Not Release to NTIS

[ ] Order From Superintendent of Documents, U.S. Government Printing Office, Washington, D.C. 20402.

[ ] Order From National Technical Information Service (NTIS), Springfield, VA. 22161

14. NO. OF PRINTED PAGES

58

15. Price

USCOMM-DC 6043-P80